nature chemistry

ARTICLES

PUBLISHED ONLINE: 14 NOVEMBER 2016 | DOI: 10.1038/NCHEM.2644

Engineering genetic circuit interactions within and between synthetic minimal cells

Katarzyna P. Adamala[1†‡], Daniel A. Martin-Alarcon[2‡], Katriona R. Guthrie-Honea[1] and Edward S. Boyden[1,2,3*]

Genetic circuits and reaction cascades are of great importance for synthetic biology, biochemistry and bioengineering. An open question is how to maximize the modularity of their design to enable the integration of different reaction networks and to optimize their scalability and flexibility. One option is encapsulation within liposomes, which enables chemical reactions to proceed in well-isolated environments. Here we adapt liposome encapsulation to enable the modular, controlled compartmentalization of genetic circuits and cascades. We demonstrate that it is possible to engineer genetic circuit-containing synthetic minimal cells (synells) to contain multiple-part genetic cascades, and that these cascades can be controlled by external signals as well as inter-liposomal communication without crosstalk. We also show that liposomes that contain different cascades can be fused in a controlled way so that the products of incompatible reactions can be brought together. Synells thus enable a more modular creation of synthetic biology cascades, an essential step towards their ultimate programmability.

Chemical systems capable of performing biochemical reactions in the absence of live cells have been used extensively in research and industry to study and model biological processes[1,2], to produce small molecules[3,4], to engineer proteins[5,6], to characterize RNAs[7], as biosensors[8,9] and molecular diagnostic tools[10], and to extend the sensing abilities of natural cells[11]. Organisms from all three domains of life have been used to obtain transcription/translation (TX/TL) extracts for cell-free production of biochemical products from genetic codes[12]. Encapsulating cell-free TX/TL extracts into liposomes creates bioreactors often referred to as synthetic minimal cells (here abbreviated as synells)[13–16]. Although synells have been employed to make functional proteins using encapsulated systems reconstituted from recombinant cell-free translation factors[17–19], as well as cell-free extracts from bacterial[6,20] and eukaryotic cells[21], work on liposomal synells has so far focused on the expression of single genes, with the goal of synthesizing a single-gene product, and within a homogeneous population of liposomes.

Here we confront a key issue in synthetic biology—the modularity of multicomponent genetic circuits and cascades. We show that by encapsulating genetic circuits and cascades within synells (Fig. 1a,b) and orchestrating the synells to either operate in parallel (Fig. 1c), communicate with one another (Fig. 1d) or fuse with one another in a controlled way (Fig. 1e), we can create genetic cascades that take advantage of the modularity enabled by liposomal compartmentalization. Thus, our strategy enables genetic cascades to proceed in well-isolated environments while permitting the desired degree of control and communication. We present design strategies to construct and utilize such synell networks, and thus expand the utility of liposome technology and improve the modularity of synthetic biology. Synell networks may support complex chemical reactions that would benefit from both the high-fidelity isolation of multiple reactions from one another, as well as controlled communication and regulatory signal exchange between those reactions. We show, for example, the controlled fusion of two populations of synells that contain mammalian transcriptional and mammalian translational machinery, which are normally incompatible when combined in the same compartment.

Results

Confinement of genetic circuits in liposomes. Before exploring the control of, and communication with, synells that contain genetic cascades, we first characterized the basic structural and functional properties of individual synells. To characterize the size and functionality of our liposomes, we labelled liposome membranes with red dye (rhodamine functionalized with a lipid tail) and filled the liposomes with cell-free TX/TL extract derived from HeLa cells[22–25], as well as DNA encoding either green fluorescent protein (GFP) or split GFP. Structured illumination microscopy (SIM) images showed that GFP liposomes had a diameter between 100 nm and 1 μm (Fig. 2a), a measurement that we confirmed with dynamic light scattering (DLS, Supplementary Fig. 1). We used flow cytometry to quantify the functional expression of genes by synells; 68.4% of the GFP liposomes expressed fluorescence, along with 61.8% of those that encapsulated split GFP (Fig. 2b–d; Supplementary Fig. 2 shows control flow-cytometry experiments). We characterized the enzymatic activity of several reporters in our liposomes (Supplementary Fig. 3) and used a western blot to provide an additional non-enzymatic characterization of luciferase expression (Supplementary Fig. 4). We compared the performance of mammalian (HeLa) and bacterial (*E. coli*) TX/TL systems in our liposomes, and found the mammalian system to be slower and have a lower protein yield (Supplementary Fig. 5).

Having established that the liposomes were of the proper size and functionality, we next sought to verify that a well-known advantage

[1]Media Lab, Massachusetts Institute of Technology, Cambridge, Massachusetts 02139, USA. [2]Department of Biological Engineering, Massachusetts Institute of Technology, Cambridge, Massachusetts 02139, USA. [3]McGovern Institute for Brain Research, Department of Brain and Cognitive Sciences, Massachusetts Institute of Technology, Cambridge, Massachusetts 02139, USA. †Present address: Department of Genetics, Cell Biology, and Development, University of Minnesota, 5-128 MCB 420 Washington Ave SE, Minneapolis, Minnesota 55455, USA. ‡These authors contributed equally to this work. *e-mail: esb@media.mit.edu

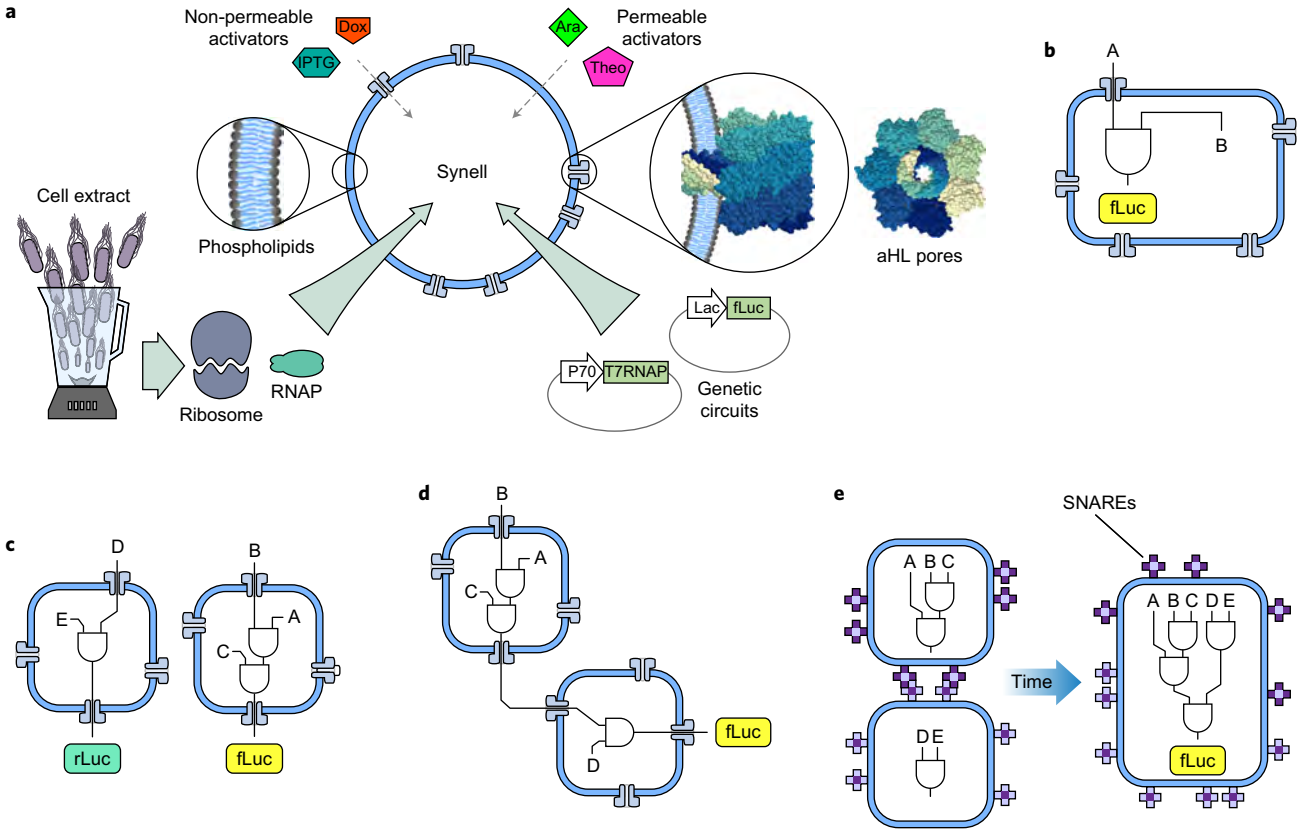

Figure 1 | An overview of genetic circuit interactions within and between synells. a, Synells are semipermeable compartments made from a phospholipid bilayer membrane and various contents. The membrane can display a variety of proteins, including channel-forming proteins such as aHL (grey membrane pores). The phospholipid membranes of synells are permeable to molecules such as theophylline (Theo) and arabinose (Ara), and are permeable to others, such as IPTG and Dox, when aHL channels are present; these molecules can be used to trigger activity within synells. Synells can encapsulate cell lysates with transcriptional and/or translational activity, as well as DNA vectors that encode genes. In this Article, we demonstrate four novel competencies of synells that, together, can be used to create complex, modular genetic circuits. **b**, Synells can contain genetic circuits in which all the components and operations take place within the same liposome. fLuc, firefly luciferase. **c**, Two genetic circuits can work independently in separate liposome populations. rLuc, Renilla luciferase. **d**, Genetic circuits within two different liposome populations can interact. **e**, Genetic circuits can run in parallel in separate compartmentalized reactions; if those reactions are encapsulated by liposomes that carry fusogenic peptides, such as SNAREs, the reaction products can be joined together in a hierarchical fashion. In panels **b**–**e**, the letters A, B, C, D and E represent inputs to genetic circuits (proteins, DNA, small molecules, and so on).

of liposomal compartmentalization—facilitated reaction efficacy caused by molecular confinement (encapsulating reactants within a liposome facilitates their interaction because of the small volume)[26–29]—can help support multicomponent genetic circuits as well as chemical reactions of higher order. We compared cell-free TX/TL reactions that produce firefly luciferase (fLuc) from one, two or three protein components, and tested them in bulk solution versus synells. In this experiment, we used HeLa-cell extract that constitutively expressed the ten–eleven translocation (Tet) protein to mediate small-molecule induction of the transcription of the one, two or three fLuc components, as well as alpha-haemolysin (aHL), which serves as a pore to admit doxycycline (Dox) to trigger Tet function[20,30,31]. The one-component luciferase was simply conventional monolithic fLuc (Fig. 3a); the two-component system (that is, to explore second-order reactions) comprised the two halves of a split fLuc, each attached to a coiled coil and a split intein fragment to bring the halves together and covalently bridge them (Fig. 3b)[32]; and the three-component system involved the halves of split fLuc bearing coiled coils and split inteins, with the coiled coils targeting a third protein, a scaffold (Fig. 3c)[32].

For all three orders of luciferase-producing reactions, the effect of dilution on fLuc expression was weaker for the liposomes than for the bulk solution (Fig. 3d–f; $P < 0.0001$ for the interaction between factors of encapsulation and dilution factor; analysis of variance (ANOVA) with factors of encapsulation and dilution factor; see Supplementary Tables 1–3 for the full statistics and Supplementary Fig. 6 for corresponding experiments under the control of a constitutive P70 promoter). As expected, fLuc expression was proportional to the concentration of Dox added to the external solution, and depended on aHL (Fig. 3g–i show end-point expression after three hours (Supplementary Fig. 7 shows the corresponding expression at a one hour end point, and Supplementary Figs 8–10 for the same reactions in bulk solution)). Liposomes produced lower amounts of fLuc than the same volume of TX/TL extract in bulk solution—probably because of the well-known property of stochastic loading of reagents into liposomes[27,28] ($P < 0.0001$ for the factor of encapsulation in ANOVA with factors of time, encapsulation and order (Supplementary Table 4 gives the full statistics)). For the third-order reaction, we found that liposome encapsulation resulted in an efficacy nearly equal to that of bulk solution (Fig. 3l; $P = 0.1324$ for the factor of encapsulation in ANOVA with factors of time and encapsulation (Supplementary Table 7 gives the full statistics)), whereas for the first-order and second-order reactions the liposomes resulted in lower efficacies (Fig. 3j,k; $P < 0.0001$ for the factor of encapsulation in ANOVAs for both analyses, each with factors of time and encapsulation (Supplementary Tables 5 and 6 give the full statistics)). Thus, molecular confinement in liposomes may help facilitate higher-order reactions that require multiple chemical building blocks to be brought together,

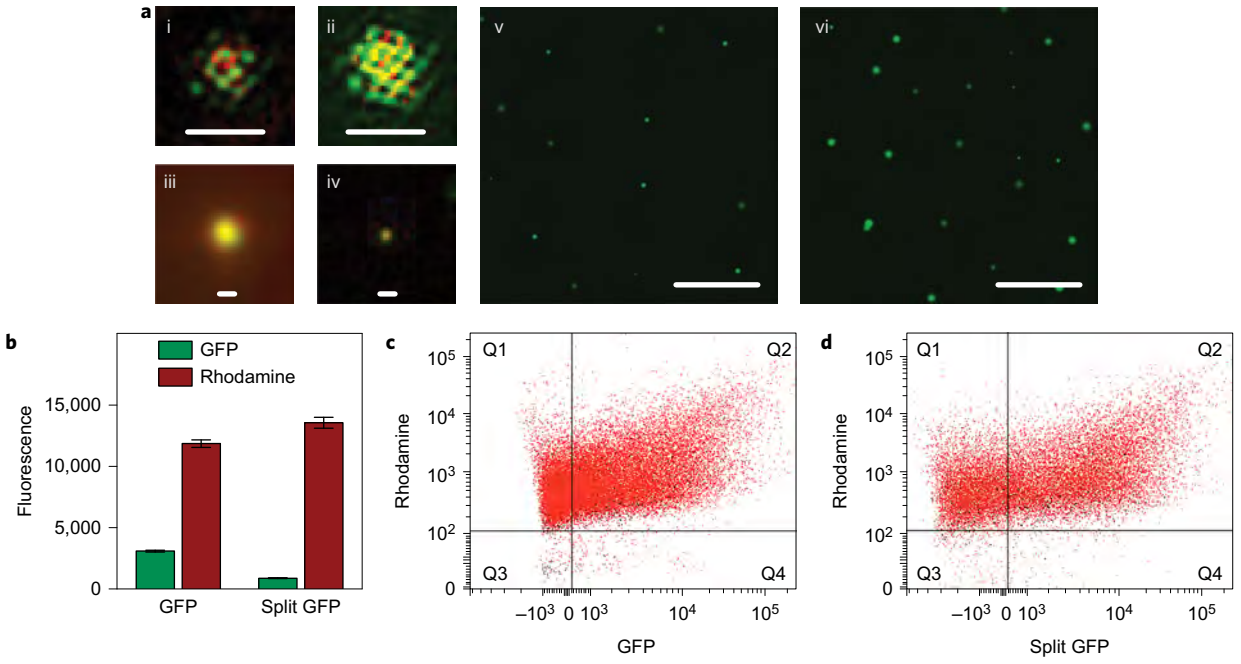

Figure 2 | Molecular confinement of multicomponent genetic cascades. a, Images of liposomes that express GFP. **i–iv**, SIM images of representative liposomes that express GFP and have membranes labelled with rhodamine. Every SIM image (**i–iv**) represents a separate liposome; all the liposomes were imaged on the same day and all the liposomes came from the same sample, prepared 24 h before imaging. All SIM images in this figure are at the same scale. Scale bars, 1 μm (**i** and **ii**) and 200 nm (**iii** and **iv**). **v**,**vi**, Widefield epifluorescent images of liposomes that express GFP. The liposomes for this imaging sample were extruded through a 2 μm filter and dialysed with a 1 μm membrane; **v** shows sample after 6 h incubation and **vi** shows an aliquot of the same sample after 24 h incubation. Scale bars, 10 μm (**v** and **vi**). **b–d**, Fraction of synells that express GFP and split GFP, measured by flow cytometry (Supplementary Fig. 2 shows the control flow-cytometry experiments). **b**, Bulk expression of GFP and fluorescence measured on the sample prior to the flow-cytometry experiments. **c**, Analysis of samples that express GFP; 68.4% of the liposomes produced a measurable green signal. **d**, Analysis of samples that expressed split GFP; 61.8% of the liposomes produced a measurable green signal.

because the restricted movement of reagents increases the probability of the requisite multiway interactions.

Insulation of genetic circuits that operate in parallel liposome populations. As a next step towards engineering sets of liposomes that can communicate with one another, we set out to determine whether liposomes could be used to insulate multiple and potentially incompatible genetic circuits from each other, so that they could operate in the same bulk environment. This insulation would enable modular design; each circuit could be optimized independently and deployed in the same environment as other circuits without interference. These circuits could reuse the same parts (proteins, DNA) for different purposes in different liposomes, and thereby circumvent one limitation of genetic circuits designed for all parts to operate within the same living cell (where one must assume that all the circuit elements might encounter each other and must therefore be inherently orthogonal). Different liposome populations could also contain chemical microenvironments that are not mutually compatible (for example, bacterial and mammalian extracts, or mammalian transcriptional and mammalian translational machinery)—there are numerous examples throughout chemistry of reactions being run under specialized, and thus often isolated, reaction conditions[33].

We first assessed whether multiple liposomal circuits could operate in parallel without crosstalk. To do this, we created populations of liposomes that could respond differently to the same external activator. We built two populations of liposomes carrying mammalian TX/TL extract and the same amount of Dox-inducible luciferase DNA (either Renilla luciferase (rLuc) or fLuc), but varied the amount of aHL DNA to result in high-aHL and low-aHL synell populations (Fig. 4a). High-aHL and low-aHL synells responded to the non-membrane-permeable Dox in the external solution, doing so proportionally to their own aHL concentrations (Fig. 4b). We observed no evidence that Dox acting on one liposome population affected the expression of luciferase in the other population—specifically, there was no significant difference in fLuc expression in high-aHL fLuc liposomes when the rLuc liposomes were high-aHL versus low-aHL, and the same held for the other combinations (Fig. 4b; Sidak's multiple comparisons test after ANOVA with factors of luciferase type and aHL combination (Supplementary Table 8 gives the full statistics, and Supplementary Figs 11 and 12 give the rLuc and fLuc expression data at different aHL plasmid concentrations, for two different time points)). That is, luciferase expression from each liposome population depended only on the amount of aHL DNA present in that population, and not on that of the other population (Fig. 4c–e). This experiment thus not only verifies the independent operation of multiple non-interacting liposomes, but also verifies that multiple liposome populations can be programmed in advance to have varying response levels to a given trigger and, subsequently, in the same internal solution, they can be triggered to function simultaneously.

Communication between genetic circuits that operate in multiple liposome populations. Having established that genetic circuits in separate populations of liposomes could operate independently, we next sought to begin to create controlled communication pathways between populations of synells. In this way we could create a compartmentalized genetic circuit—which, as noted above, may need to be separated from others for reasons of control fidelity, toxicity or reagent tunability—and connect it to other compartmentalized circuits. Although previous work has emphasized the importance of modularity in genetic circuits[34], to

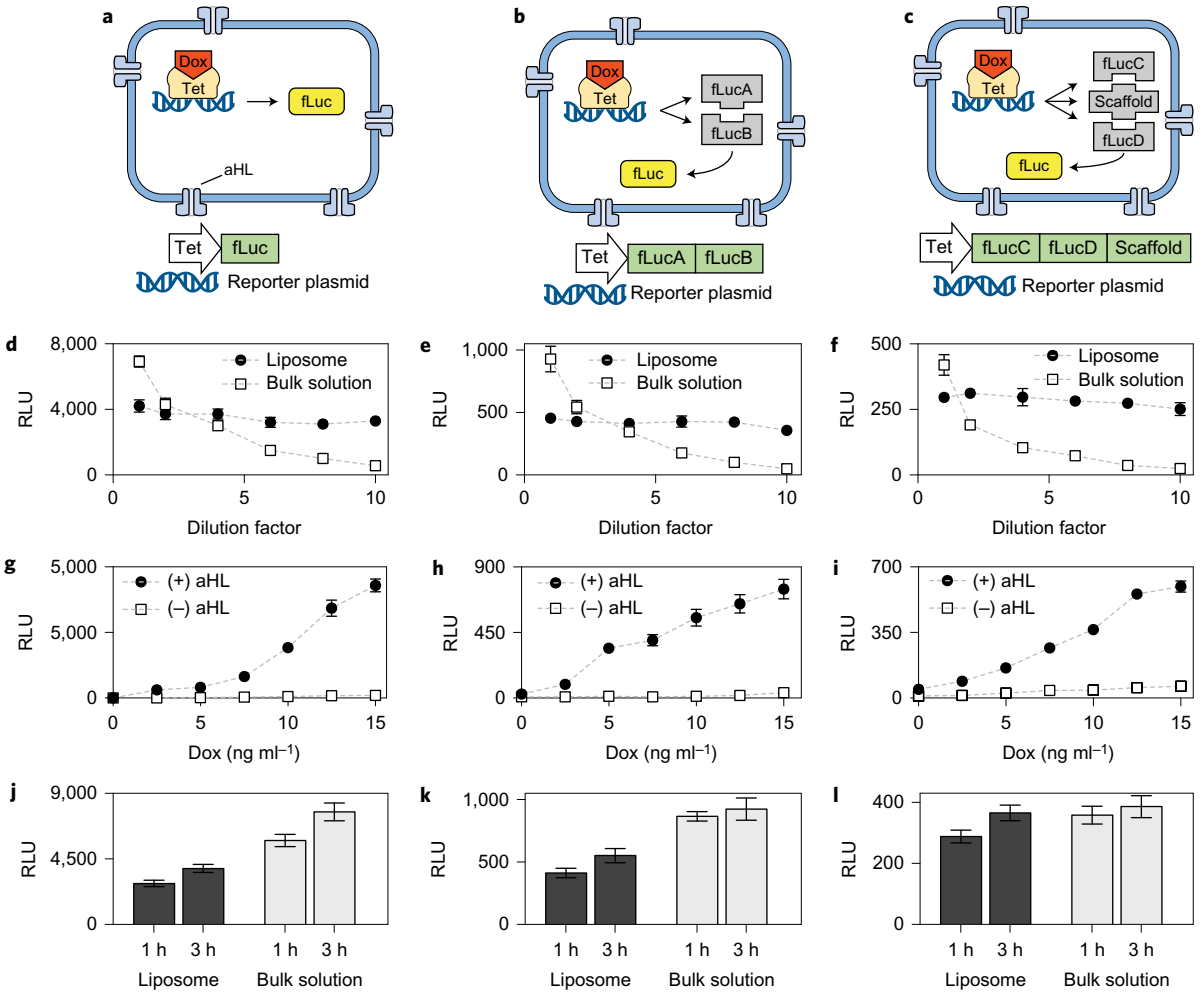

Figure 3 | Comparison of single- and multicomponent genetic circuits. a–c, Genetic cascades that involve one-, two- or three-part luciferase protein assemblies. Expressed under Dox-inducible Tet promoters were whole fLuc (**a**), the two halves (here denoted fLucA and fLucB) of split-fLuc-bearing split inteins and mutually binding coiled coils (**b**) and two halves (here denoted fLucC and fLucD) of split-fLuc-bearing split inteins and coiled coils that bind to a third common template (denoted 'scaffold') (**c**). **d–f**, Effects of dilution on fLuc expression in liposomes versus bulk solution for the fLuc assemblies described in **a–c** (Supplementary Fig. 6 shows the experiments under the control of a constitutive P70 promoter). Dotted lines throughout this figure are visual guides, not fits. **g–i**, End-point expression of luciferase, measured at the 3 h time point, for seven different concentrations of Dox. Supplementary Fig. 7 gives the corresponding 1 h end-point expression data, and Supplementary Figs 8–10 gives these for the same reactions in bulk solution. **j–l**, Comparison of liposomal versus bulk solution expression of luciferase, at two different time points and for 10 ng ml^{-1} of Dox. The two plasmids in **k** and three plasmids in **l** were mixed at equimolar ratios, with the total DNA concentration held constant. Error bars indicate s.e.m., $n = 4$ replicates.

our knowledge nobody has approached the problem by physically separating circuit elements into different liposomes. We built two-component circuits by mixing together two populations of liposomes, a 'sensor' that senses an external small-molecule cue and a 'reporter' that receives a message from the sensor population and produces an output; we could vary the occupancy of each population to achieve a different overall ratio of the two components (Fig. 5a (Supplementary Fig. 13 shows additional characterizations of the membrane-permeable small molecules used throughout Fig. 5a, and Supplementary Tables 9 and 10 give the associated statistics)). Our first version was built with bacterial TX/TL extract (Fig. 5b). The sensor liposomes contained IPTG (isopropyl-β-D-thiogalactoside, a small, non-membrane-permeable activator that induces the *lac* promoter) and the arabinose-inducible gene for aHL (arabinose is membrane permeable, unlike IPTG); these liposomes thus sensed arabinose and released IPTG by expressing aHL channels. We combined these with reporter liposomes that contained constitutively expressed aHL, in which fLuc was under the control of the *lac* promoter—either directly (fLuc under the *lac* promoter) or indirectly (T7RNAP under the *lac* promoter and fLuc under the T7 promoter)—and found that multicomponent compartmentalized genetic circuits thus constructed were able to operate as coherent wholes.

We tested both systems with multiple dilutions of the sensor and reporter liposomes, and found similar dose–response curves from titration of either species of liposome (Fig. 5c,d; bars in these panels represent final time points of six hours; for the complete time series that includes the data in Fig. 5c, see Supplementary Fig. 14; for the end-point expression of the circuit in Fig. 5c without arabinose triggering, see Supplementary Fig. 15; for the complete time series that includes the data in Fig. 5d, see Supplementary Fig. 16; for the end-point expression of the circuit in Fig. 5d without arabinose triggering, see Supplementary Fig. 17). Using this modular architecture, we constructed a genetic circuit that combines both bacterial and mammalian components (Fig. 5e). The sensor liposome in this case responded to theophylline (membrane permeable) to release Dox (non-membrane-permeable). Dox, in turn, activated fLuc expression in the reporter liposomes built with mammalian components. As before, we showed that the multicompartment genetic cascade could function

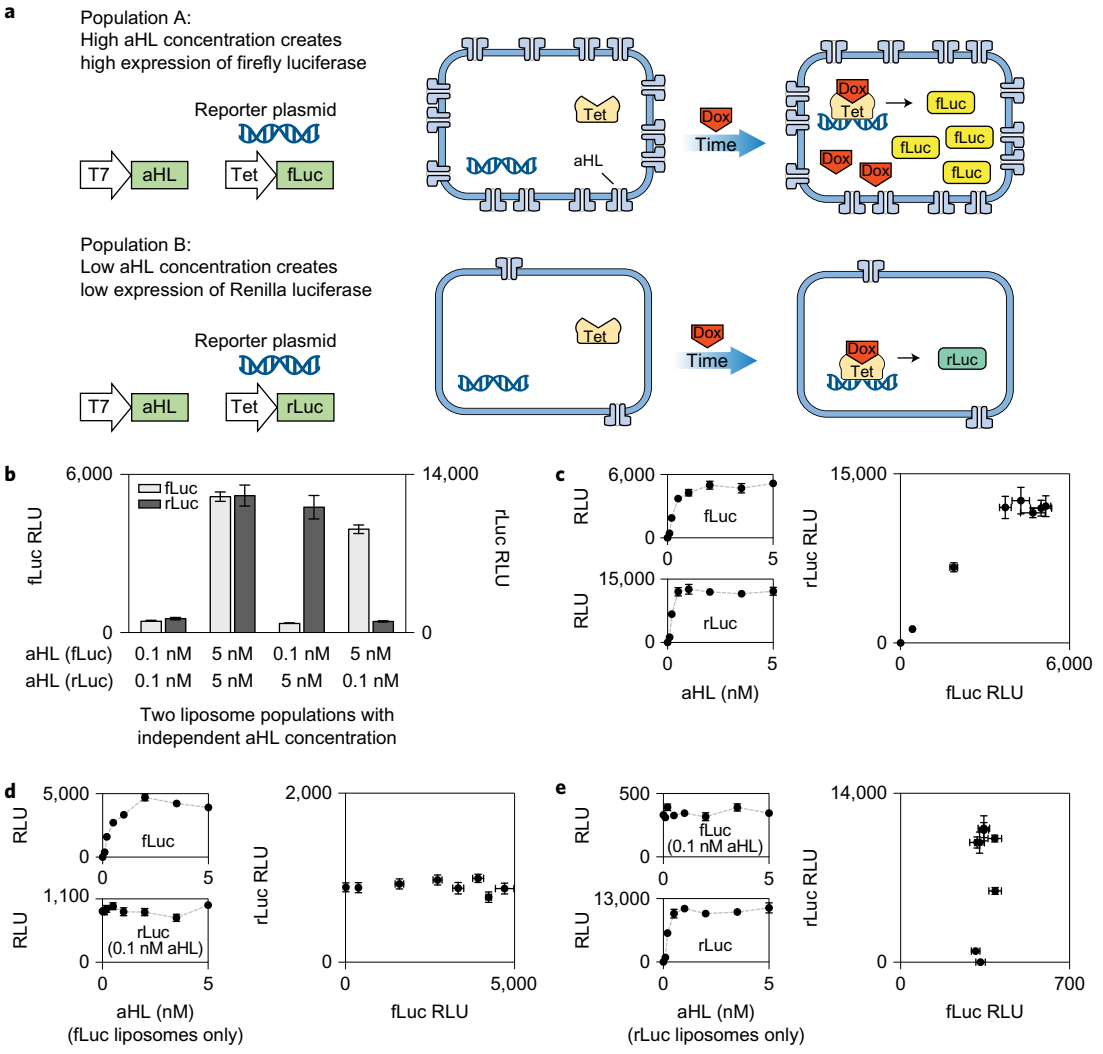

Figure 4 | Insulation of genetic circuits that operate in parallel liposome populations. a, Schematic of liposome populations designed to contain similar genetic components, but to respond differently to the same environmental concentration of the non-membrane-permeable small-molecule activator Dox, by expressing different amounts of the aHL channel protein. These liposomes contain a measured amount of the plasmid for constitutively expressed aHL, and of a plasmid that drives either fLuc or rLuc from the Tet-inducible promoter (the luciferase plasmids were always held at the same concentration). For all the data in this figure, the two populations were incubated together in the solution containing Dox and harvested after 6 h (Supplementary Figs 11 and 12 give the rLuc and fLuc expression as a function of aHL plasmid concentration after 2 and 6 h, respectively). **b**, Each liposome contains either 0.1 or 5 nM of the aHL plasmid. **c**, Luciferase expression in symmetrical populations in which the amount of aHL DNA is the same across the two populations; the amount of fLuc and rLuc expression is shown in the graphs with respect to aHL plasmid concentration and to each other. **d**,**e**, Luciferase expression in asymmetrical populations. **d**, Luciferase expression when Renilla liposomes have a constant aHL plasmid concentration (0.1 nM), but the concentration of that plasmid is varied in the firefly liposomes. The expressions of rLuc and fLuc are shown in the graphs against the plasmid concentration in firefly liposomes and against each other. **e**, Luciferase expression as in **d**, but with constant aHL plasmid concentration in firefly liposomes and variable concentration in Renilla liposomes. Error bars indicate s.e.m., $n = 4$ replicates.

as designed, with similar fLuc expression dose–response curves on titrating either the sensor or reporter liposome concentration (Fig. 5f; bars in this panel represent final time points of six hours; for the complete time series that includes the data in Fig. 5f, see Supplementary Fig. 18; for the end-point expression of the circuit in Fig. 5f without theophylline triggering, see Supplementary Fig. 19). Thus, even multicomponent genetic circuits with different chemical microenvironments (for example, made from bacterial versus mammalian cell extracts) can be assembled into coherent networks that comprise multiple modules.

Fusion of complementary genetic circuits. Finally, having established that it is possible to maintain liposomes in high-integrity states despite being mixed, we sought to engineer synells to fuse so that they could bring together two genetic cascades into the same environment in a programmable fashion. Two precursors might require synthesis in different milieus, but ultimately need to be reacted with one another. One prominent example is that of mammalian transcription and translation. Functionally, mixed mammalian transcription and translation cell-free extracts are not able to result in the transcription of DNA into RNA and then the translation of RNA into protein, perhaps because the microenvironments of the mammalian nucleus and cytoplasm are quite different, which makes their cell-free extracts incompatible (Supplementary Fig. 20). Rather than mixing the two cell-free extracts into a single non-functioning mixture, it might be preferable to use synells to compartmentalize the reactions. Once nuclear-extract synells have completed transcription, it might be desirable to fuse them with cytoplasmic-extract synells for the translation to take place.

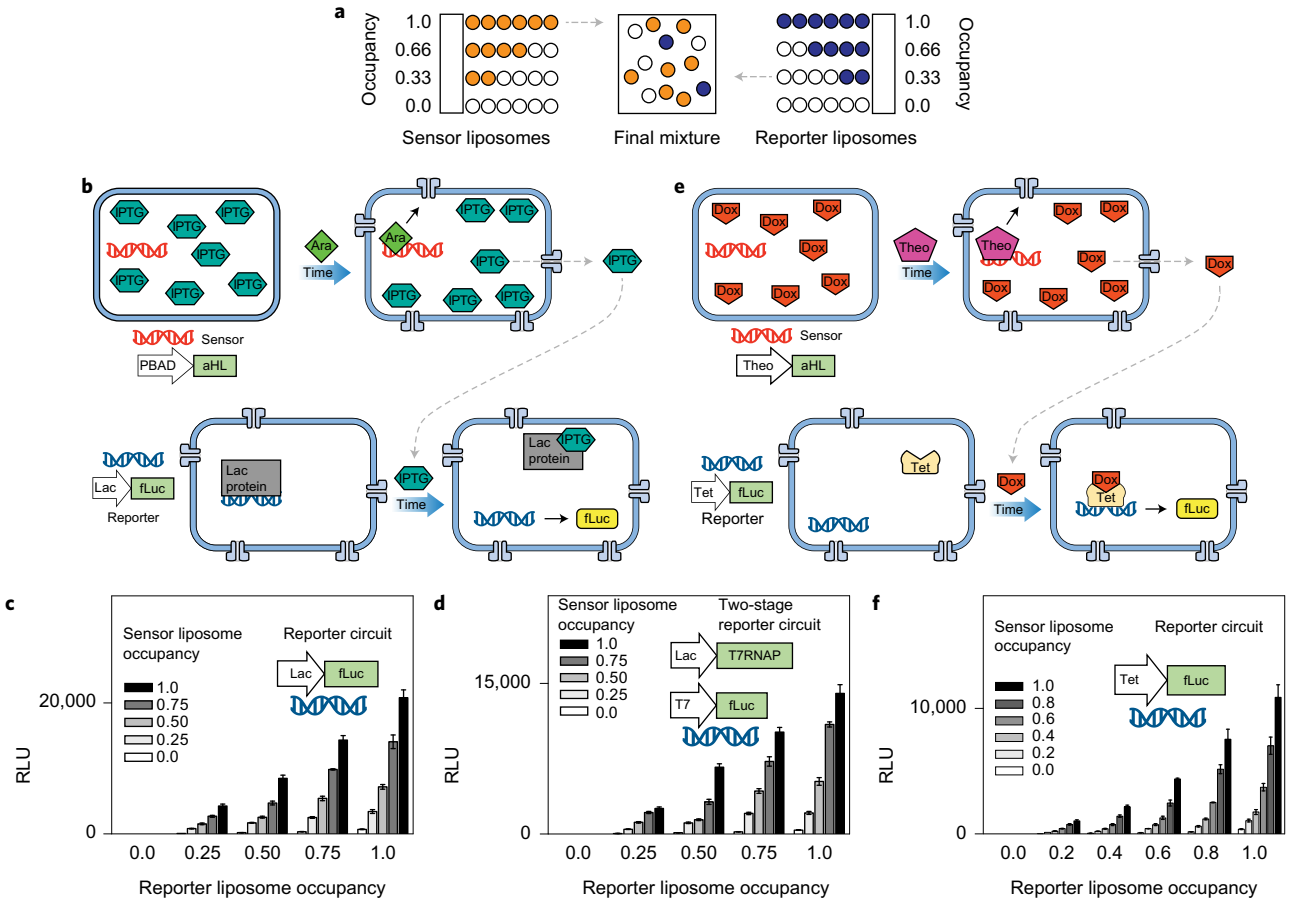

Figure 5 | Communication between genetic circuits that operate in multiple liposome populations. a, Scheme for mixing two populations of liposomes at different ratios of their components while maintaining a constant lipid concentration of 10 mM (the same scheme was used throughout this figure and in Fig. 6). Each population contains the same amount of liposomes, but the liposome occupancy can vary between 0 (all liposomes are empty) and 1 (the maximum fraction of the liposomes contain reagents). **b**–**d**, Externally activated two-part circuits, with bacterial TX/TL. **b**, Scheme of interacting populations, denoted sensor and reporter. Sensor liposomes contain the aHL gene and are filled with IPTG; reporter liposomes contain machinery for fLuc expression. During activation, arabinose (Ara) diffuses through the sensor liposome membrane and induces aHL expression, which releases IPTG, which induces fLuc expression in the reporter. **c**, Expression of fLuc for varying ratios of occupancy (as in **a**) for the sensor and reporter liposomes with the indicated contents. **c** represents the 6 h time point (Supplementary Fig. 14 shows the complete time series and Supplementary Fig. 15 shows this circuit without arabinose). **d**, Expression of fLuc for a circuit in which the reporter liposomes contain DNA for a multicomponent genetic cascade, as indicated. **d** represents the 6 h time point (Supplementary Fig. 16 shows the complete time series and Supplementary Fig. 17 shows this circuit without arabinose). **e**,**f**, Externally activated two-part circuits that contain both bacterial and mammalian TX/TL components. **e**, Sensor vesicles contain the Theo-triggered aHL gene and Dox; reporter liposomes contain constitutively expressed aHL and Tet, and Dox/Tet-driven fLuc. During activation, Theo diffuses through the membrane of the activator liposomes and induces aHL expression, which creates pores that release Dox from the activator. Dox induces fLuc expression in the reporter liposomes. **f**, Expression of fLuc for varying ratios of sensor and reporter liposomes (**f** represents the 6 h time point; Supplementary Fig. 18 gives the complete time series and shows this circuit without Theo). Error bars indicate s.e.m., $n = 4$ replicates.

Thus, we sought to make liposomes capable of controlled fusion (Fig. 6a). Fusing liposomes of opposite charge was previously demonstrated to activate gene expression in liposomes[35]. Our system uses only one kind of membrane composition (POPC (1-palmitoyl-2-oleoyl-*sn*-glycero-3-phosphorylcholine) cholesterol membranes, known to be a good environment for membrane channels such as aHL), so to achieve fusion between liposomes we used SNARE (SNAP receptor (SNAP, soluble *N*-ethylmaleimide-sensitive factor attachment protein))/coiled-coil hybrid proteins (here the hybrid proteins are called SNAREs for short), which can be generated in complementary pairs that are specific in their fusion properties[36,37]. We could thus fuse together complementary circuit elements by encapsulating them in separate populations of SNARE-fusable liposomes. We confirmed that SNAREs mediated liposome fusion through SIM imaging (Fig. 6a) by observing fluorescence resonance energy transfer (FRET) signals from lipid dyes added to the liposome membranes (FRET signals showed that the fusion process takes place within minutes (Supplementary Figs 21 and 22)) and by observing mixing of the liposome content, reported as dequenching of a molecular beacon encapsulated in one population of liposomes by a complementary target encapsulated in the other population (Supplementary Fig. 23). We observed large liposomes and also liposome aggregates (presumably in the process of fusing) of sizes on the order of 5–10 μm, and measured a minimal amount of leakage from the liposomes during the process of fusion (Supplementary Fig. 24).

We tried several combinations of complementary circuit elements: the gene for T7RNAP and a T7-driven fLuc (Fig. 6b); a non-membrane-permeable small-molecule trigger (IPTG) and an IPTG-triggered (*lac*-promoter-driven) fLuc (Fig. 6c); genes for a membrane pore (aHL) and a *lac*-promoter-driven fLuc in an IPTG-containing ambient (Fig. 6d); and two different genes encoding for parts of split luciferase using the same fLucA and fLucB as in Fig. 3b (Fig. 6e). For one final test, liposomes that carried

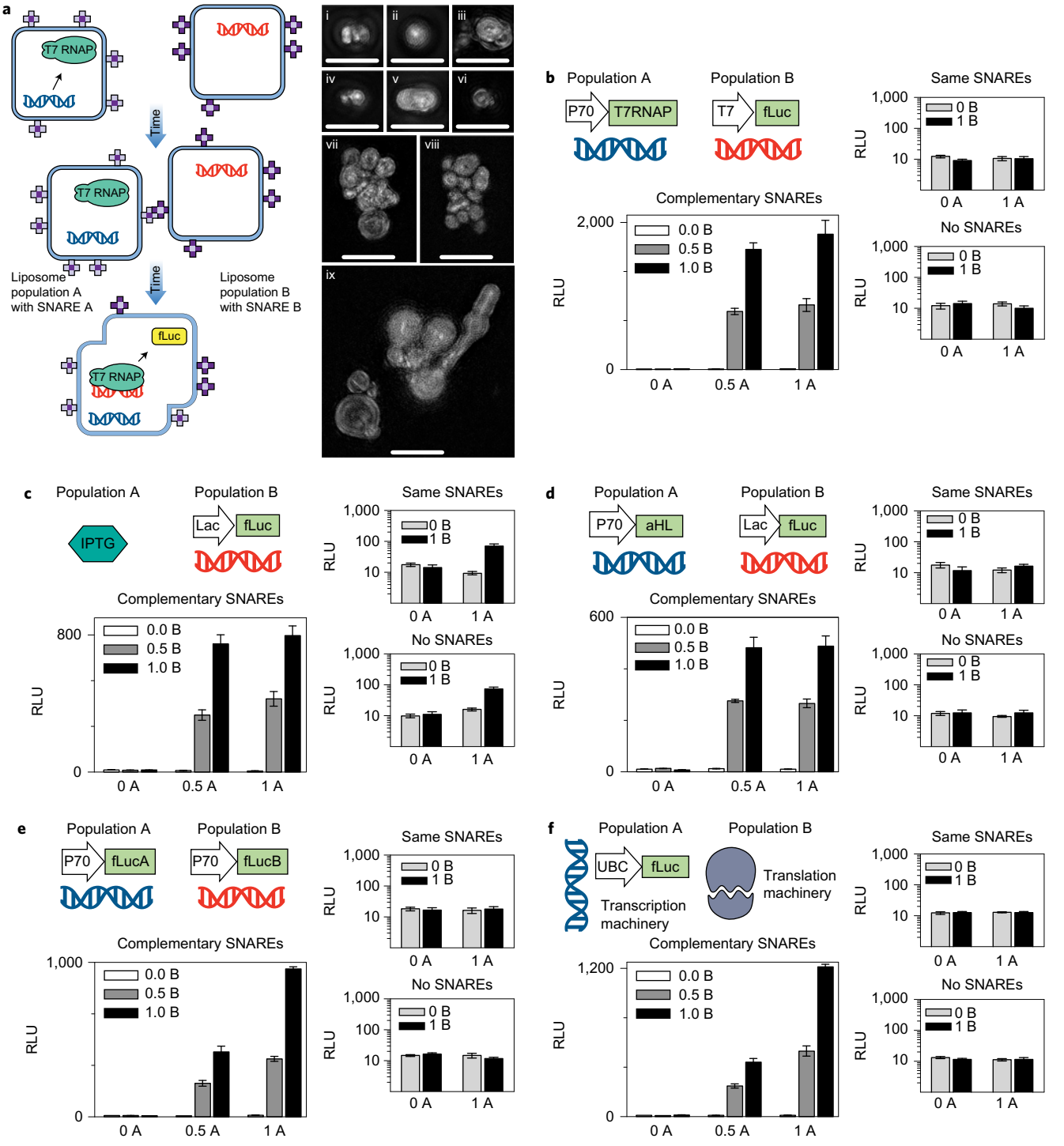

Figure 6 | Fusion of complementary genetic circuits. a, General scheme for SNARE-mediated liposome fusion. We created two populations of liposomes, A and B, decorated with complementary SNARE protein mimics in their outer leaflet. The images to the right, in **i**–**ix**, are maximum-intensity projections of SIM *z*-stacks of liposome membrane labelled with rhodamine, bearing complementary SNARE pairs and fused for 4 h. All the images (**i**–**ix**) represent separate fields of view. Scale bars, 5 μm. All liposomes in this figure, except **f**, contained bacterial TX/TL components. **b**–**f**, Five different types of the liposome fusion concept, exploring several ways to distribute genetic circuits across fusable liposomes, with two different populations of liposomes at three occupancy levels for each case. **b**, Mixing of constitutively expressed T7 RNA polymerase with fLuc under T7 promoter. **c**, Mixing of a non-membrane-permeable small-molecule activator IPTG with its inducible promoter driving fLuc production. **d**, Mixing of a constitutively expressed membrane channel with an inducible promoter driving fLuc production in the background of the small molecule that induces the promoter (IPTG). **e**, Mixing liposomes with genes that encode split protein. **f**, Mixing liposomes that contain a mammalian transcription (HeLa) and translation (HeLa) system, producing fLuc. For all five systems in **b**–**f**, the large graph shows experiments in which the two liposome populations had matching SNAREs, the top small panel is when both liposomes had the same SNARE, and the bottom one when neither population had any SNAREs. In both small graphs of **b**–**f**, the *y* axis is a logarithmic scale to show the near-zero values for non-fusing liposomes. Switching which liposome contained which SNARE had no effect on the results (Supplementary Fig. 25), whereas the absence of SNARE proteins or the presence of identical SNAREs on both populations hindered fusions (small graphs in **b**–**f**). Error bars indicate s.e.m., $n = 4$ replicates.

mammalian nuclear (transcription) extract and the gene for fLuc, incubated for 12 hours, were then mixed with liposomes that contained cytoplasmic (translation) extract, and further incubated for 12 hours (Fig. 6f). We were able to observe the production of fLuc protein, even though a direct combination of transcriptional and translational machinery produced no fLuc above background levels (Supplementary Fig. 20). Throughout all these cases, we observed production of the final output of the genetic cascade only when the two liposome populations were equipped with SNAREs, and only when they were a SNARE cognate pair ($P < 0.0001$ for the factor of SNARE compatibility, ANOVA with factors of mechanism, occupancy and SNARE compatibility (Supplementary Table 11 gives the full statistics; for systems in this figure, switching which liposome contained which SNARE had no effect on the results, as shown in Supplementary Fig. 25)).

Discussion. Liposomes are key in chemistry and chemical biology for compartmentalizing chemical reactions that require different environments or act on different samples. In this work, we show how synells—liposomes containing genes as well as transcriptional and/or translational machinery—enable a great level of modularity for genetic circuit design and execution. We showed that circuits could be designed to run in synell populations in the same container, independent of each other because of the insulation provided by the liposomal membrane. Genetic circuits could also be connected to communicate with one another through small-molecule messengers. This communication was possible even across liposomes that contained incompatible microenvironments, as we showed by constructing the first genetic circuit to contain bacterial and mammalian cell-free extracts and genetic elements. Finally, we explored the use of SNARE mimics to fuse synells together, enabling the direct union of separately synthesized reaction components. Using this strategy, we were able to produce RNA encoding for fLuc in one population of liposomes that contained mammalian transcriptional extract, which on fusion with liposomes that contained mammalian translational extract resulted in protein production—an outcome that does not occur if the gene is simply added to a mixture of the two extracts.

Synells thus enable a new level of modularity for synthetic biology. Modularity is key in engineering, because breaking a complex synthetic biology system into parts that can be independently controlled or regulated, without crosstalk, and that communicate only in well-defined ways, enables each part to be optimized individually while supporting their incorporation into an emergent whole. Our technologies will enable a large number of different synthetic biology problems to be made modular, even those that involve genetic cascades that might interfere with each other (or pose toxicity issues) if they were to all occur in one pot. As our method of compartmentalization is liposomal, there is no need for specialized hardware to mediate the communication and control of multiple interacting reaction systems. Precise temporal control of synell networks could be enhanced even further by using light to trigger optogenetic signalling cascades, which in turn can trigger downstream effects[38,39]. We also show that the molecular confinement of liposomes can facilitate multicomponent protein–protein interactions.

Our synells, in addition to the power they offer to synthetic biology, may also enable the simulation of various complex behaviours that have been proposed as characteristics of early life forms. Controlled communication between cells, the fusion of genetic elements across cells and the assembly of complex genetic cascades towards defined cellular behaviours are all traits that arose in the course of early evolution. Synells have been widely used as models for studying the origin and earliest evolution of life[40–44]. For example, one of us has previously shown that liposomes encapsulating a simple catalyst can be used to model early Darwinian competition mechanisms[41]. Interacting encapsulated genetic circuits will hopefully enable the study of the more-complex characteristics that have been proposed for the last universal common ancestor[45–47], and perhaps help to reveal the dynamic and boundary conditions that underlie the mechanisms of Darwinian evolution[48,49].

Materials

Cloning of expression constructs. The P70 (OR2-OR1-Pr (ref. 50)) and *lac* (Llac-0-1 (ref. 51)) promoter constructs were used in a modified pCI vector (Promega). The original promoter region of the vector was replaced by the appropriate promoter to make our constructs[51]. For bacterial expression, the previously described transcription terminator T500 was added at the end of each ORF (open reading frame). The original untranslated region (UTR) was also removed and replaced with the previously described UTR1 (ref. 50). The mammalian Tet constructs were built into the Tet-On 3G bidirectional vector (Clontech) by cloning the genes into MCS1. The araBAD constructs were built using a PBAD vector[52] (Thermo). We used PBAD–hisB and removed the His-tag and the enterokinase recognition site prior to inserting the genes used in this study.

Flow cytometry with GFP and split GFP. The fluorescence signal from these GFP liposomes was measured after 12 h of incubation for the experiments in Fig. 2b–d. Membranes (red fluorescence) were labelled with Lissamine rhodamine B 1,2-dihexadecanoyl-*sn*-glycero-3-phosphoethanolamine triethylammonium salt (rhodamine DHPE), used at 0.2 molar percentage of the POPC concentration. GFP was expressed from a plasmid with the T7 promoter. The halves of split GFP were fused to complementary coiled coils and expressed from two different plasmids (both with the T7 promoter). For the flow-cytometry analysis, events in two fluorescent channels were analysed: GFP and red fluorescence. Each dataset consists of a minimum of 19,000 events. Figure 2c shows an analysis of liposomes that expressed GFP and Fig. 2d shows an analysis of liposomes that expressed split GFP. The percentage of liposomes that expressed protein was calculated as the percentage of events in the quadrant positive in both the green and red channels (Q2 on both plots). The flow cytometer was not calibrated using size standards, and therefore all the information about the size of the particles in the experiment is approximate. For the detailed size measurements of the liposomes in this work, Supplementary Fig. 1 gives data from the DLS experiments. The flow-cytometry analysis was performed on a FACSCanto II, and the data analysis was performed using a FACSDiva 8.0.

fLuc assays. fLuc activity was assayed using the Steady-Glo Luciferase Assay System (Promega). The protein analysis was performed according to the manufacturer's instructions. The cell lysis protocol was replaced with a modified procedure for lysing liposome-encapsulated expression reactions. The 50 µl liposome reactions were quenched by 10 µl of Quench Mix that contained 0.3% v/v Triton-X100 (to disrupt the vesicles), TURBO DNAse (Thermo; final concentration ~2U per 60 µl; 1 µl used), TURBO DNAse buffer (final concentration ~0.5×, 2.5 µl 10× stock used), RNase Cocktail Enzyme Mix (mixture of RNAse A and RNAse T1, 3 µl per 60 µl reaction (Thermo)). The samples were incubated with the Quench Mix for 15 min at 37 °C. The resulting sample was used directly with the Steady-Glo luciferase assay, according to the manufacturer's instructions.

The result is given in relative light units (RLU) with a 10 s integration time.

Enzyme activity assays. Renilla, NanoLuc luciferase, beta-lactamase, beta-galactosidase and chloramphenicol acetyltransferase activity were assayed using commercially available kits, according to the manufacturer's instructions (Supplementary Information gives the detailed procedures).

***E. coli* cell-free TX/TL extract.** Our *E. coli* cell-free extract was prepared according to the Noireaux Lab protocol, from Rosetta 2 BL21 cells (Novagen)[50,53]. The entire extract preparation was performed in a cold room (4 °C).

HeLa cell-free extract. The HeLa cell-free translation extract was prepared according to a previously published protocol[24]. The entire extract preparation was performed in a cold room (4 °C). For the mammalian *in vitro* transcription, we used the HeLa cell-free nuclear fraction transcription system HeLaScribe (Promega).

SNARE protein mimics. The SNARE protein mimics were chemically synthesized by solid-phase protein synthesis (Genscript). SNARE-A was a fusion of the E3 coiled-coil motif and the transmembrane region of the VAMP2 protein (residues 85–116). SNARE-B was a fusion of the K3 coiled-coil motif with a transmembrane region from the syntaxin-1A protein (residues 258–288), as described before[36]. The SNARE peptide-to-lipid molar ratio used in all the experiments was 1:500.

Liposomes that undergo SNARE-mediated fusion form large aggregates made from multiple starter liposomes[36,37]; this does not affect the results in Fig. 6, but it would probably reduce the molecular confinement effects observed in Fig. 3.

Received 6 December 2015; accepted 12 September 2016; published online 14 November 2016

References

1. Carlson, E. D., Gan, R., Hodgman, C. E. & Jewett, M. C. Cell-free protein synthesis: applications come of age. *Biotechnol. Adv.* **30,** 1185–1194 (2012).
2. Smith, M. T., Wilding, K. M., Hunt, J. M., Bennett, A. M. & Bundy, B. C. The emerging age of cell-free synthetic biology. *FEBS Lett.* **588,** 2755–2761 (2014).
3. Hodgman, C. E. & Jewett, M. C. Cell-free synthetic biology: thinking outside the cell. *Metab. Eng.* **14,** 261–269 (2012).
4. Miller, D. & Gulbis, J. Engineering protocells: prospects for self-assembly and nanoscale production-lines. *Life* **5,** 1019–1053 (2015).
5. Shimizu, Y., Kuruma, Y., Ying, B.-W., Umekage, S. & Ueda, T. Cell-free translation systems for protein engineering. *FEBS J.* **273,** 4133–4140 (2006).
6. Shin, J. & Noireaux, V. An *E. coli* cell-free expression toolbox: application to synthetic gene circuits and artificial cells. *ACS Synth. Biol.* **1,** 29–41 (2012).
7. Takahashi, M. K. *et al.* Rapidly characterizing the fast dynamics of RNA genetic circuitry with cell-free transcription–translation (TX-TL) systems. *ACS Synth. Biol.* **4,** 503–515 (2015).
8. Michener, J. K., Thodey, K., Liang, J. C. & Smolke, C. D. Applications of genetically-encoded biosensors for the construction and control of biosynthetic pathways. *Metab. Eng.* **14,** 212–222 (2012).
9. Vamvakaki, V. & Chaniotakis, N. A. Pesticide detection with a liposome-based nano-biosensor. *Biosens. Bioelectron.* **22,** 2848–2853 (2007).
10. Pardee, K. *et al.* Paper-based synthetic gene networks. *Cell* **159,** 940–954 (2014).
11. Lentini, R. *et al.* Integrating artificial with natural cells to translate chemical messages that direct *E. coli* behaviour. *Nat. Commun.* **5,** 4012 (2014).
12. Zemella, A., Thoring, L., Hoffmeister, C. & Kubick, S. Cell-free protein synthesis: pros and cons of prokaryotic and eukaryotic systems. *Chem. Bio. Chem.* **16,** 2420–31 (2015).
13. Forster, A. C. & Church, G. M. Towards synthesis of a minimal cell. *Mol. Syst. Biol.* **2,** 45 (2006).
14. Brea, R. J., Hardy, M. D. & Devaraj, N. K. Towards self-assembled hybrid artificial cells: novel bottom-up approaches to functional synthetic membranes. *Chem. Pub. Soc. Euro.* **21,** 12564–12570 (2015).
15. Luisi, P. L., Ferri, F. & Stano, P. Approaches to semi-synthetic minimal cells: a review. *Naturwissenschaften* **93,** 1–13 (2006).
16. Stano, P. & Luisi, P. L. Semi-synthetic minimal cells: origin and recent developments. *Curr. Opin. Biotechnol.* **24,** 633–638 (2013).
17. Murtas, G., Kuruma, Y., Bianchini, P., Diaspro, A. & Luisi, P. L. Protein synthesis in liposomes with a minimal set of enzymes. *Biochem. Biophys. Res. Commun.* **363,** 12–17 (2007).
18. Yu, W. *et al.* Synthesis of functional protein in liposome. *J. Biosci. Bioeng.* **92,** 590–593 (2001).
19. Oberholzer, T., Nierhaus, K. H. & Luisi, P. L. Protein expression in liposomes. *Biochem. Biophys. Res. Commun.* **261,** 238–241 (1999).
20. Noireaux, V. & Libchaber, A. A vesicle bioreactor as a step toward an artificial cell assembly. *Proc. Natl Acad. Sci. USA* **101,** 17669–17674 (2004).
21. Stech, M. *et al.* Production of functional antibody fragments in a vesicle-based eukaryotic cell-free translation system. *J. Biotechnol.* **164,** 220–231 (2012).
22. Weber, L. A, Feman, E. R. & Baglioni, C. A cell free system from HeLa cells active in initiation of protein synthesis. *Biochemistry* **14,** 5315–5321 (1975).
23. Wimmer, E. Cell-free, *de novo* synthesis of poliovirus. *Science.* **254,** 1647–1651, (1991).
24. Mikami, S., Masutani, M., Sonenberg, N., Yokoyama, S. & Imataka, H. An efficient mammalian cell-free translation system supplemented with translation factors. *Protein Expr. Purif.* **46,** 348–357 (2006).
25. Mikami, S., Kobayashi, T., Masutani, M., Yokoyama, S. & Imataka, H. A human cell-derived *in vitro* coupled transcription/translation system optimized for production of recombinant proteins. *Protein Expr. Purif.* **62,** 190–198 (2008).
26. Tan, C., Saurabh, S., Bruchez, M. P., Schwartz, R. & Leduc, P. Molecular crowding shapes gene expression in synthetic cellular nanosystems. *Nat. Nanotechnol.* **8,** 602–608 (2013).
27. de Souza, T. P. *et al.* Encapsulation of ferritin, ribosomes, and ribo-peptidic complexes inside liposomes: insights into the origin of metabolism. *Orig. Life Evol. Biosph.* **42,** 421–428 (2012).
28. de Souza, T. P., Fahr, A., Luisi, P. L. & Stano, P. Spontaneous encapsulation and concentration of biological macromolecules in liposomes: an intriguing phenomenon and its relevance in origins of life. *J. Mol. Evol.* **79,** 179–192 (2014).
29. Caschera, F. & Noireaux, V. Integration of biological parts toward the synthesis of a minimal cell. *Curr. Opin. Chem. Biol.* **22,** 85–91 (2014).
30. Stefureac, R., Long, Y. T., Kraatz, H. B., Howard, P. & Lee, J. S. Transport of α-helical peptides through α-hemolysin and aerolysin pores. *Biochemistry* **45,** 9172–9179 (2006).
31. Gouaux, E., Hobaugh, M. & Song, L. α-Hemolysin, γ-hemolysin, and leukocidin from *Staphylococcus aureus*: distant in sequence but similar in structure. *Protein Sci.* **6,** 2631–2635 (1997).
32. Selgrade, D. F., Lohmueller, J. J., Lienert, F. & Silver, P. A. Protein scaffold-activated protein trans-splicing in mammalian cells. **135,** 7713–7719 (2013).
33. Tu, Y. *et al.* Mimicking the cell: bio-inspired functions of supramolecular assemblies. *Chem. Rev.* **116,** 2023–2078 (2016).
34. Del Vecchio, D., Ninfa, A. J. & Sontag, E. D. Modular cell biology: retroactivity and insulation. *Mol. Syst. Biol.* **4,** 161 (2008).
35. Caschera, F. *et al.* Programmed vesicle fusion triggers gene expression. *Langmuir* **27,** 13082–13090 (2011).
36. Meyenberg, K., Lygina, A. S., van den Bogaart, G., Jahn, R. & Diederichsen, U. SNARE derived peptide mimic inducing membrane fusion. *Chem. Commun.* **47,** 9405–9407 (2011).
37. Robson Marsden, H., Korobko, A. V., Zheng, T., Voskuhl, J. & Kros, A. Controlled liposome fusion mediated by SNARE protein mimics. *Biomater. Sci.* **1,** 1046–1054 (2013).
38. Inglés-Prieto, Á. *et al.* Light-assisted small-molecule screening against protein kinases. *Nat. Chem. Biol.* **11,** 952–954 (2015).
39. Boyden, E. S. A history of optogenetics: the development of tools for controlling brain circuits with light. *F1000 Biol. Rep.* **3,** 11 (2011).
40. Hanczyc, M. M., Fujikawa, S. M. & Szostak, J. W. Experimental models of primitive cellular compartments: encapsulation, growth, and division. *Science* **302,** 618–622 (2003).
41. Adamala, K. & Szostak, J. W. Competition between model protocells driven by an encapsulated catalyst. *Nat. Chem.* **5,** 495–501 (2013).
42. Balaram, P. Synthesizing life. *Curr. Sci.* **85,** 1509–1510 (2003).
43. Adamala, K. *et al.* Open questions in origin of life: experimental studies on the origin of nucleic acids and proteins with specific and functional sequences by a chemical synthetic biology approach. *Comput. Struct. Biotechnol. J.* **9,** e201402004 (2014).
44. Ruiz-Mirazo, K., Briones, C. & de la Escosura, A. Prebiotic systems chemistry: new perspectives for the origins of life. *Chem. Rev.* **114,** 285–366 (2014).
45. Glansdorff, N., Xu, Y. & Labedan, B. The last universal common ancestor: emergence, constitution and genetic legacy of an elusive forerunner. *Biol. Direct* **3,** 29 (2008).
46. Woese, C. The universal ancestor. *Proc. Natl Acad. Sci. USA* **95,** 6854–6859 (1998).
47. Theobald, D. L. A formal test of the theory of universal common ancestry. *Nature* **465,** 219–222 (2010).
48. Spencer, A. C., Torre, P. & Mansy, S. S. The encapsulation of cell-free transcription and translation machinery in vesicles for the construction of cellular mimics. *J. Vis. Exp.* **80,** e51304 (2013).
49. Adamala, K., Engelhart, A. E., Kamat, N. P., Jin, L. & Szostak, J. W. Construction of a liposome dialyzer for the preparation of high-value, small-volume liposome formulations. *Nat. Protoc.* **10,** 927–938 (2015).
50. Shin, J. & Noireaux, V. Efficient cell-free expression with the endogenous *E. coli* RNA polymerase and sigma factor 70. *J. Biol. Eng.* **4,** 8 (2010).
51. Lutz, R. & Bujard, H. Independent and tight regulation of transcriptional units in *Escherichia coli* via the LacR/O, the TetR/O and AraC/I1-I2 regulatory elements. *Nucleic Acids Res.* **25,** 1203–1210 (1997).
52. Guzman, L. M., Belin, D., Carson, M. J. & Beckwith, J. Tight regulation, modulation, and high-level expression by vectors containing the arabinose PBAD promoter. *J. Bacteriol.* **177,** 4121–4130 (1995).
53. Sun, Z. Z. *et al.* Protocols for implementing an *Escherichia coli* based TX-TL cell-free expression system for synthetic biology. *J. Vis. Exp.* **79,** e50762 (2013).

Acknowledgements

We thank E. Vasile and F. Chen for help with the SIM microscopy, and G. Paradis and K. Piatkevich for help with the flow-cytometry experiments. We thank N. Kamat and L. Jin for help with troubleshooting the DLS machine. We thank J. Szostak for sharing the liposome encapsulation formula. We thank V. Noireaux, A. Mershin and A. Engelhart for helpful discussions about cell-free TX/TL systems. E.S.B. acknowledges, for funding, the National Institutes of Health (NIH) 1U01MH106011, Jeremy and Joyce Wertheimer, NIH 1RM1HG008525, the Picower Institute Innovation Fund, NIH 1R01MH103910, NIH 1R01NS075421, National Science Foundation CBET 1053233, New York Stem Cell Foundation-Robertson Award and NIH Director's Pioneer Award 1DP1NS087724. D.A.M.-A. acknowledges support from the Janet and Sheldon Razin (1959) Fellowship.

Author contributions

K.P.A. and D.A.M.-A. contributed equally to this work. K.P.A., D.A.M.-A. and K.R.G.-H. performed the experiments. K.P.A., D.A.M.-A. and E.S.B. designed experiments, analysed the data and wrote the manuscript.

Additional information

Supplementary information is available in the online version of the paper. Reprints and permissions information is available online at www.nature.com/reprints. Correspondence and requests for materials should be addressed to E.S.B.

Competing financial interests

K.P.A., D.A.M.-A. and E.S.B. submitted a provisional patent application based on this work.

nature chemistry

SUPPLEMENTARY INFORMATION

DOI: 10.1038/NCHEM.2644

In the format provided by the authors and unedited.

Supplementary information

For the article "Engineering genetic circuit interactions within and between synthetic minimal cells"

by Katarzyna P. Adamala, Daniel A. Martin-Alarcon, Katriona R. Guthrie-Honea, Edward S. Boyden

Supplementary Methods

Sources of materials and product characterization

The vectors used in this work were synthesized in house, from oligonucleotide gBlocks from IDT (IDT DNA, Coralville, IA, US) or DNA oligo building blocks from Epoch (Epoch Life Science Inc., Sugar Land, TX, US). The sequence of all plasmids was confirmed by Sanger Sequencing by Eton Bioscience Inc. (San Diego, CA, US) or Quintara Bio (Boston, MA, US). Unless otherwise stated, small molecules, activators and buffer components, were purchased either form Sigma Aldrich (St. Louis, MO, US) or Thermo Fisher (Waltham, MA, US) and were used without further purification. All antibiotics used for cloning and TL/TL preparation were purchased from GoldBio (Olivette, MO, US) and used without further purification. All experiments were performed in buffers prepared using RNAse free water from Ambion (sold by Thermo Fisher). The lipids used fo liposome formation were purchased from Avanti Polar Lipids (Alabaster, AL, US) and were used without further purification.

The enzyme products obtained in cell-free reactions were characterized with commercially available detection kits: Renilla, NanoLuc and Firefly luciferases using products from Promega (Madison, WI, US); Beta-lactamase, Chloramphenicol acetyltransferase and Beta-galactosidase using product from Thermo Fisher (Waltham, MA, US).

Liposome preparation

Our procedure for preparing liposomes was based on previously published protocols, most notably with the specific modifications described by the Mansy Lab[11,48]. Briefly, a chloroform solution of 20 mg (26 µmol) of POPC (Avanti Polar Lipids) and 20 mg (52 µmol) of cholesterol (Avanti Polar Lipids) was evaporated into a thin film using a round bottom flask. 4 mL of DEPC-treated nuclease-free water was added to the flask and vigorously vortexed for ~3 minutes. The liposome solution (~6.5 mM) was then homogenized with a hand-held homogenizer (IKA) for ~1 minute. The mixture was divided into 150 µL aliquots (~1 µmol of lipid each) and lyophilized until dry.

To prepare the final experimental liposome solution, aliquots of lyophilized lipids were hydrated with buffer containing the cell-free TX/TL extract, DNA, and small molecule activators for each experiment, to the final volume of 50 µL per reaction (~20 mM liposomes). Liposomes were extruded through a 1 µM polycarbonate track-etched membrane (Whatman). The unencapsulated solutes were removed from liposomes through dialysis using a liposome dialyzer as described previously[49], with a 0.5 mL volume slide-a-lyzer chamber and a 0.4 µM pore size polycarbonate track-etched membrane (Whatman). The dialysis was performed at 4°C. The samples were dialyzed 5 times against Dialysis Buffer (50 mM HEPES, pH=7.6, 100 mM KCl, 10 mM $MgCl_2$ and ~10mM empty and unlabeled POPC-cholesterol liposomes), with a buffer change every 10 minutes and 3 additional buffer changes every 20 minutes.

Renilla luciferase assays

Renilla luciferase (rLuc) activity was assayed using the Renilla Luciferase Assay System (Promega). Liposome reactions were stopped using Quench Mix according to the procedure described in section "Firefly luciferase assays" of **Materials and Methods**. The resulting sample was used directly with the Renilla luciferase assay, according to the manufacturer's instructions. The result is given in RLU—relative light units with 10 s integration time.

NanoLuc luciferase assays

NanoLuc luciferase activity was assayed using the Nano-Glo Luciferase Assay System (Promega). Liposome reactions were stopped using Quench Mix according to the procedure described in section "Firefly luciferase assays" of Materials and Methods. The resulting sample was used directly with the Nano-Glo luciferase assay, according to the manufacturer's instructions.

Beta-lactamase assays

Beta-lactamase activity was assayed using the LyticBLAzer-FRET B/G assay kit (Thermo). Liposome reactions were stopped using Quench Mix according to the procedure described in section "Firefly luciferase assays" of Materials and Methods. The resulting sample was used directly with the beta-lactamase assay, according to the manufacturer's instructions.

Beta-galactosidase assays

Beta-galactosidase activity was assayed using the β-Gal Assay Kit (Thermo). Liposome reactions were stopped using Quench Mix according to the procedure described in section "Firefly luciferase assays" of **Materials and Methods**. The resulting sample was used directly with the beta-galactosidase assay, according to the manufacturer's instructions.

Chloramphenicol acetyltransferase assays

Chloramphenicol acetyltransferase activity was assayed using the FAST CAT Green (Deoxy) Chloramphenicol Acetyltransferase Assay Kit (Thermo). Liposome reactions were stopped using Quench Mix according to the procedure described in section "Firefly luciferase assays" of **Materials and Methods**. Samples were then heated to 65°C for 10 minutes, to inactivate endogenous acetylating enzymes[1]. The resulting samples were used directly with the FAST CAT assay according to the manufacturer's instructions. GR ACS Silica Gel Grade 12 28-200 Mesh plates (EMD Millipore) were used for product analysis. After visualization, the product and substrate spots were scraped from the plate and mixed with 0.35 mL of methanol per spot. The samples were centrifuged for 1 min, a 200 µL aliquot of each methanol solution was removed, and the fluorescence of both substrate and product was quantified (excitation 490 mm, emission 525 mm).

Supplementary Discussion

Nomenclature

We use "liposomes", "synells", and "synthetic minimal cells" interchangeably throughout this paper. There is no universally acknowledged definition of synthetic minimal cells in the literature[2–6]. We understand synells as liposome bioreactors performing some of the biochemical functions of the living cell, most notably transcription and translation for the expression of proteins.

Expression of enzymatic reporter proteins in synthetic minimal cells

We focused on enzymatic reporters to measure protein expression in all our experiments, for these reporters can be quantitatively detected at very low concentrations, and with linear ranges that extend over several orders of magnitude[7–9]. We expressed firefly luciferase (fLuc), Renilla luciferase (rLuc), Nano-Luc luciferase[10], beta lactamase, beta galactosidase, and chloramphenicol acetyltransferase in liposomes, using the constitutively active P70 bacterial promoter (**Fig S3**). We assayed their enzymatic activity as a proxy for protein concentration, using multiple batch reactions run in parallel and collected at different time points. All five enzymatic reporters expressed well in synells.

The full list of all tested enzymatic reporter proteins, corresponding small molecule substrates, and expression profiles in cell-free bacterial system under T7 promoter is shown in **Fig. S3**. In addition to the luciferase activity luminescence assays, the identity of expressed firefly luciferase protein was confirmed using Western Blot analysis, **Fig. S4**.

Optimization of sequences for the theophylline riboswitch

It has been previously noted that putative ribosome binding sites (RBSs) inside the gene of interest might bypass the theophylline aptamer, resulting in expression of truncated genes independently of the theophylline riboswitch activity[11]. We screened the sequence of [P70][Theo][T7RNAP] for putative ribosome binding sites, using the sequence composition and spacing rules elucidated by Lentini et al[12]. Using the [T7][fLuc] reporter, we validated that T7RNAP expression is indeed under the control of the

theophylline riboswitch—with an amount of "leakage" comparable to previously reported levels[11] (see **Fig. S13b**).

Encapsulation efficiency and size distribution

The efficiency of solute encapsulation inside POPC liposomes of a given radius r (nm) at a given concentration c (mM) can be estimated using this formula, used in the Szostak Laboratory and empirically confirmed by encapsulation experiments :

%internal volume = vol_liposome*liposomes_ml*10^-19

Where:

vol_liposome = (4/3)*Pi*(r^3)

is the volume of the lumen of a single liposome, in nm^3;

liposomes_ml = surface_area_ml/area_liposome

is the number of liposomes per 1 mL;

surface_area_ml = (c*10^-6)*((760*10^21)/0.9*N_A)/2.5)/2

is the surface area of liposomes per 1 mL of solution of a given c (mM), with POPC MW=760 and length of the lipid bilayer approximated to 2.5nm; N_A is Avogadro's number;

and finally,

area_liposome = 4*Pi*(r^2)

is the surface area of the liposome outer leaflet, in nm^2.

These calculations were made with the assumption that liposome curvature is negligible, so the inner and outer leaflet contain an equal number of lipids and have equal surface area. The thickness of the bilayer was approximated at 2.5 nm[13]. The addition of cholesterol increases bilayer thickness up to 30%, thus affecting the encapsulation rate[14], but we cannot reliably estimate the influence of cholesterol on packing density and surface area of the liposomes. According to this formula, a 25 mM solution of 200 nm POPC liposomes will contain ~14% of the total volume encapsulated inside liposomes. In reality, the encapsulation rate of liposomes used in our experiments is likely lower. This is due to factors like the presence of cholesterol in POPC membranes and the fact, that in liposomes extruded through, e.g., a 200 nm filter, the size distribution of liposomes varies greatly and is, on average, smaller than 200nm[15–17]. The differences in yield of protein synthesis inside synthetic cells, explained by the difference in efficiency of encapsulating the TX/TL enzyme mix, have been observed before.[18]

We used DLS to analyze samples of liposomes prepared according to the protocol used in this work (see **Materials and Methods** and **Fig. S1**). The liposome sample size distribution is consistent between different preparations (samples from separate encapsulation, extrusion and dialysis processes, prepared on different days, are compared). The DLS experiments are very sensitive to fluorescent dyes present in the solution; therefore, we chose to perform those experiments on samples not producing any fluorescent reporter protein.

Efficiency of small molecule activator transfer

To assess the efficiency of IPTG activation between liposomes, we estimated the release of small molecules from liposomes through aHL channels. We prepared a sample of IPTG sensor liposomes like in experiments in **Fig. 5c**, but also containing 100 mM calcein—a fluorescent, non-membrane-permeable, small-molecule dye. Thus, the sensor liposomes contained both small molecules (IPTG and calcein) and the arabinose-inducible gene for aHL. We mixed these sensor liposomes 1:1 with reporter liposomes like those from **Fig. 5c** and incubated the mixture with arabinose. After incubation, we measured luciferase activity from half the liposome mixture and purified the other half on a Sepharose 4B size exclusion column, measuring the total fluorescence of the collected unencapsulated fraction. The concentration of the unencapsulated calcein, calculated from the dye fluorescence, was 0.18 mM in the 2.1 ml of the free dye fraction collected from the purification column. This corresponds to a concentration of ~3.78 mM in the original 100 µL sample of mixed liposomes; this can serve as an estimate of the concentration of small molecules that easily and maximally permeate through the aHL

pore (e.g., of IPTG). For reference, the initial concentration of IPTG and calcein in the liposome encapsulation mixture was 100 mM.

We performed an additional validation of this estimate for equilibrium IPTG concentration in the sensor-reporter mixture. We prepared a sample of reporter liposomes identical to those from **Fig. 5c**, and mixed it with empty liposomes plus IPTG to the final concentration of 3.78 mM. From this mixture we recorded a final luciferase activity of 28868 RLU (average of 3 samples, S. E. M. 815 RLU), which is comparable to the 20820 RLU recorded for the 1:1 mix of sensor and reporter liposomes in **Fig. 5c**.

We have further confirmed the insertion of the alpha hemolysin channel into the bilayer membrane of liposomes by two separate experiments. For the first experiment, we prepared the aHL as a fusion to the fluorescent protein mClover. We expressed the mClover-aHL fusion in large unilamellar vesicles prepared with Lissamine Rhodamine B (red fluorescent dye tethered to a phospholipid: 1,2-Dihexadecanoyl-sn-Glycero-3-Phosphoethanolamine, Triethylammonium Salt) in the phospholipid membrane. Direct confocal microscopy observation confirmed the co-localization of the green signal from the alpha hemolysin protein fusion with the red signal from the lipid-bound membrane dye (**Fig. S26**). For the second experiment, we prepared liposomes (as described in **Materials and Methods**) with two membrane dyes capable of FRET (Fluorescence Resonance Energy Transfer): Lissamine™ Rhodamine B 1,2-Dihexadecanoyl-sn-Glycero-3-Phosphoethanolamine, Triethylammonium Salt and NBD-PE N-(7-Nitrobenz-2-Oxa-1,3-Diazol-4-yl)-1,2-Dihexadecanoyl-sn-Glycero-3-Phosphoethanolamine, Triethylammonium Salt. Alpha hemolysin protein was expressed inside liposomes, from a constitutive bacterial P70 promoter, using bacterial TX/TL extract. The decrease in the observed FRET signal (increase in donor fluorescence and decrease in receptor fluorescence) indicated changes in the surface area of the liposome. This technique has been previously used to see insertion of biomolecules into the bilayer membrane of liposomes[19]. The observed increase of the membrane surface area is attributed to the insertion of the membrane protein into the bilayer. The negative control experiment, expressing firefly luciferase—a soluble protein with no known association to phospholipid membranes, results in no change of FRET signal over time.

Cascaded circuits

Cascaded circuits, in which the product of one gene triggers the production of the next, are useful for a variety of reasons—for signal amplification (i.e., a relatively small input signal can trigger a high

output), for modularity (e.g., a variety of sensors can be connected to a given output), and to enable multi-node control at various points within the network (as in the configuration of natural signaling and metabolic pathways in cells, where many reagents must be regulated in timing and concentration, for efficient synthesis). Such cascaded circuits are widely employed in synthetic circuits for these reasons[20,21]. We built cascaded circuits in this experiment using liposomes with *E. coli* TX/TL extract. The circuit we constructed had the gene for fLuc (in single component form) under a T7 promoter (recognized by T7 RNA Polymerase, T7RNAP), with the gene for T7RNAP itself under the control of a membrane-permeable activator (**Fig. S13a**), here either theophylline (Theo, which activates an aptamer sequence in the 5'-UTR that un-masks a ribosome binding site and triggers protein production) or arabinose (Ara, which induces the PBAD promoter). These activators had been previously tested in phospholipid liposomes for the induction of single genes[11,22].

We found the theophylline system to be leaky, as others have observed before[11] (expression for all time points after t = 3 h was significantly different from that at t = 0, $P < 0.0001$ in Sidak's multiple comparison test, after ANOVA with factors of time and presence or absence of theophylline; **Figs. S13b** and **S13c**; see **Table S9** for full statistics). We found no measurable activation of PBAD in the absence of arabinose, suggesting that arabinose may be a useful external trigger for cascaded genetic circuits (expression for all time points was equal to that for t = 0, $P > 0.9999$ in Sidak's multiple comparison test, after ANOVA with factors of time and presence or absence of arabinose; **Figs. S13d** and **S13e**; see **Table S10** for full statistics). Additionally, researchers using theophylline have observed the need for screening their genes against putative aptamer sequences[11], to avoid naturally-occurring aptamers interacting with theophylline enough to interfere with translation and produce truncated proteins. Arabinose avoids this problem entirely; furthermore, the PBAD promoter is used in a great variety of commercially available bacterial expression vectors, many of which could be directly utilized in synells. Thus, arabinose shows great promise as a permeable activator for future liposomal genetically cascaded circuits.

Direct comparison of bacterial and mammalian systems

Synells containing mammalian and bacterial TX/TL, both systems expressing firefly luciferase, were compared side-by-side. The mammalian system was slower to reach maximum protein yield, and the total product yield was significantly lower, for the same volume and the same initial plasmid concentration (**Fig. S5**).

Typically, eukaryotic systems offer better folding and access to post-translational modifications, at the price of significantly lower yields[23]. Prokaryotic systems generally allow for higher yields at lower cost. If multi-domain proteins, complex signaling cascades, or large proteins are needed, eukaryotic systems generally should be used. Folding of large fusion proteins may be much more efficient in eukaryotic systems[24]. Also, eukaryotic systems typically offer a much wider range of post-translational modifications than prokaryotic extracts[25]. Bacterial extract, most commonly prepared form *E. coli*, is robust to changes in reaction temperature and tolerant to chemical additives while offering high yield of simple, unmodified proteins. Additionally, the bacterial TX/TL extract is relatively easy and cheap to prepare[26–30].

Mammalian cell-free TX/TL systems have been developed to synthesize long, complex proteins that require folding chaperones and post-translational modifications[23]. Commercially available rabbit reticulocyte systems offer cap-independent translation and contain mammalian folding chaperones. The glycosylation of proteins is possible in this system upon addition of canine pancreatic microsomal membranes; this typically decreases the overall yield of protein synthesis. Human HeLa cell extract is also commercially available; it is used to express antibodies, as well as large and complex proteins and viruses[31,32].

In summary, here is a brief general comparison of bacterial and mammalian systems (information based on several sources[23,28,33–35]; of course, these are generalities, and these rules of thumb may not always hold in all conditions):

	Bacterial	**Mammalian**
Protein yield	High yields	Low yields
Post-translational modifications	Very limited	Glycosylation possible, other modifications also possible
Cost of use	Low	High
Ease of use (tolerance to additives, temperature, etc.)	High: tolerance to extreme temperatures and small molecule additives	Low: narrower set of temperatures, sensitive to changes in conditions and composition of reaction mixture

Supplementary Figures

Fig. S1

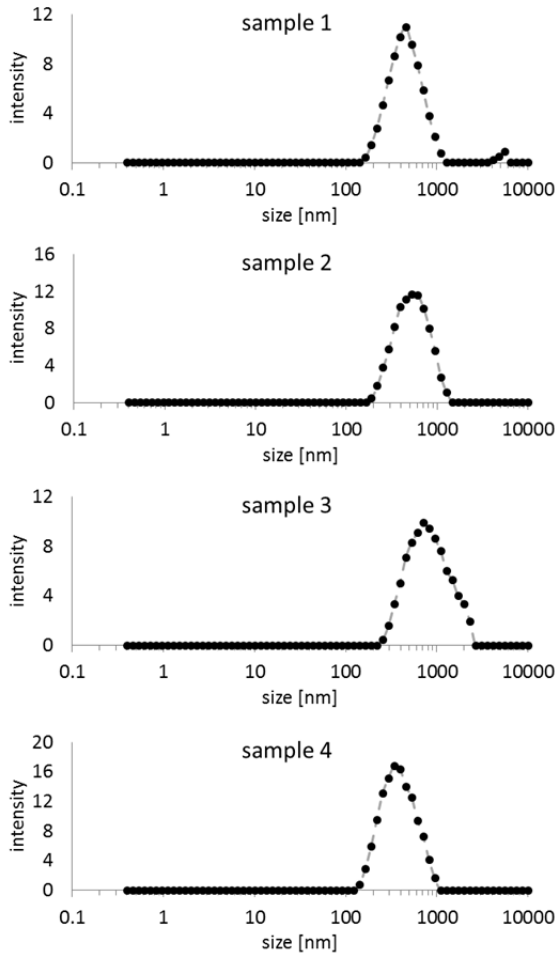

Fig. S1. Dynamic light scattering analysis of liposomes. We compared samples from separate encapsulation, extrusion and dialysis processes, prepared on different days. The measurements were performed using a Malvern Zetasizer Nano instrument, and data was analyzed using Zetasizer Ver. 7.04. All measurements were performed at 25°C, at measurement angle 173° backscatter.

Fig. S2

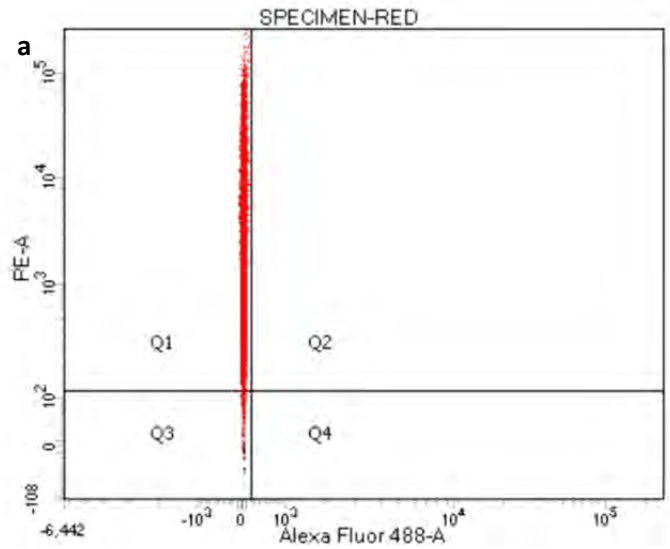

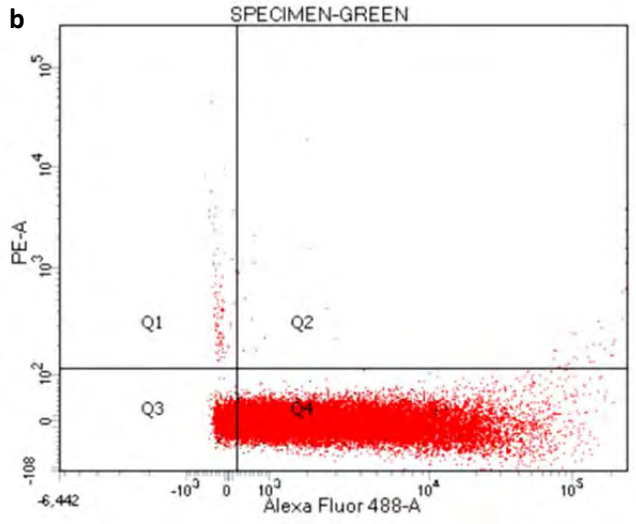

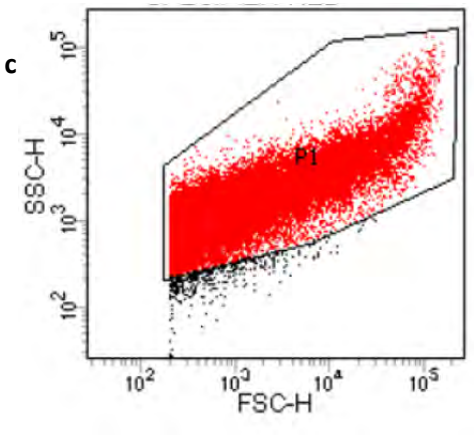

Fig. S2. Control samples for flow cytometry of synthetic minimal cells (as in **Figs. 2c** and **2d**). All samples contained liposomes with cell-free TX/TL mixture and a plasmid for expressing GFP, encapsulated in liposomes labeled with rhodamine-bearing membrane dye (red) prepared as described in **Materials and Methods**. **a.** Control red fluorescence sample: liposomes membrane-labeled with Lissamine Rhodamine B, without the GFP plasmid. The y-axis is fluorescence in the red (rhodamine) channel and the x-axis is fluorescence in the green (GFP) channel. **b.** Control green fluorescence sample: liposomes with T7-GFP plasmid; axes are as in **a**. Reaction conditions and plasmid concentrations are the same as in **Fig. 2**. The cytometry analysis was performed on FACSCanto II, and the data analysis was performed using FACSDiva 8.0. The red dots on the cytometry data on this figure and in **Fig. 2** represent counted events; the black dots represent events below the scattering threshold P1 (the threshold was set by the operator to eliminate events smaller than the typical size of dust in the sample); the same threshold applied to all datasets. **c.** Example of the scattering threshold size range; the y-axis is side scatter SSC-H and the x-axis is forward scatter FSC-H.

Fig. S3

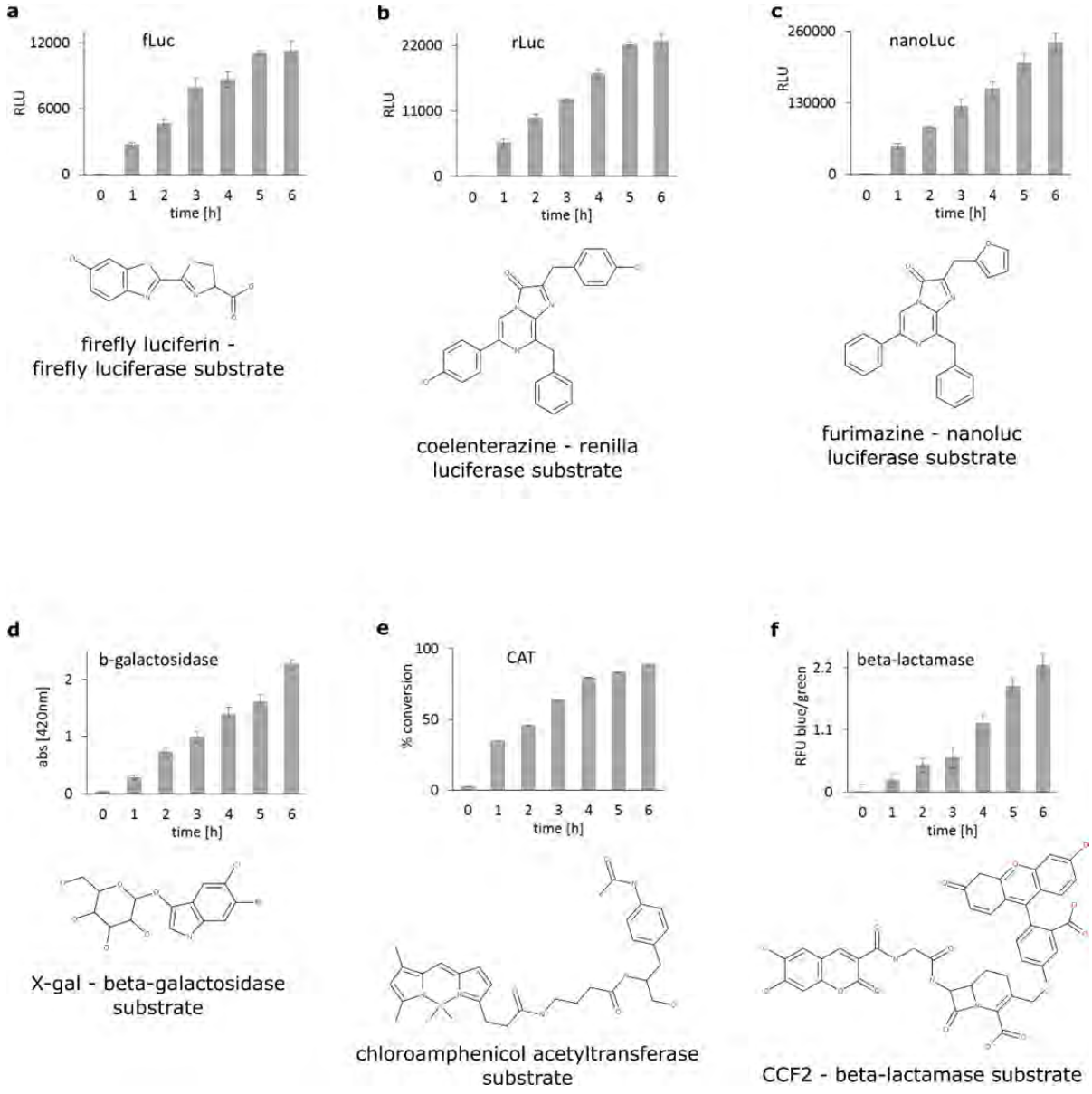

Fig. S3. T7-driven expression of enzymatic reporter proteins in synthetic cells. For each system, the substrate for the enzyme is also shown. **a.** Firefly luciferase. **b.** Renilla luciferase. **c.** NanoLuc luciferase. **d.** β-Galactosidase. **e.** Chloramphenicol acetyltransferase. **f.** β-lactamase. All constructs were under the P70 promoter, expressed in bacterial cell-free TX/TL extract according to the procedure described in **Materials and Methods**. All 6 enzymes were analyzed according to the protocols from the assay kits

used for each enzyme—see **Materials and Methods** for details. Each reaction was stopped at the indicated time point and processed according to the protocol for each enzyme assay kit. Error bars in panels **a, b, c,** and **d** indicate S. E. M., error bars in panels **e** and **f** indicate error propagated from the standard deviation of two wavelength signals. All data points are an arithmetic average of 3 replicates.

Fig. S4

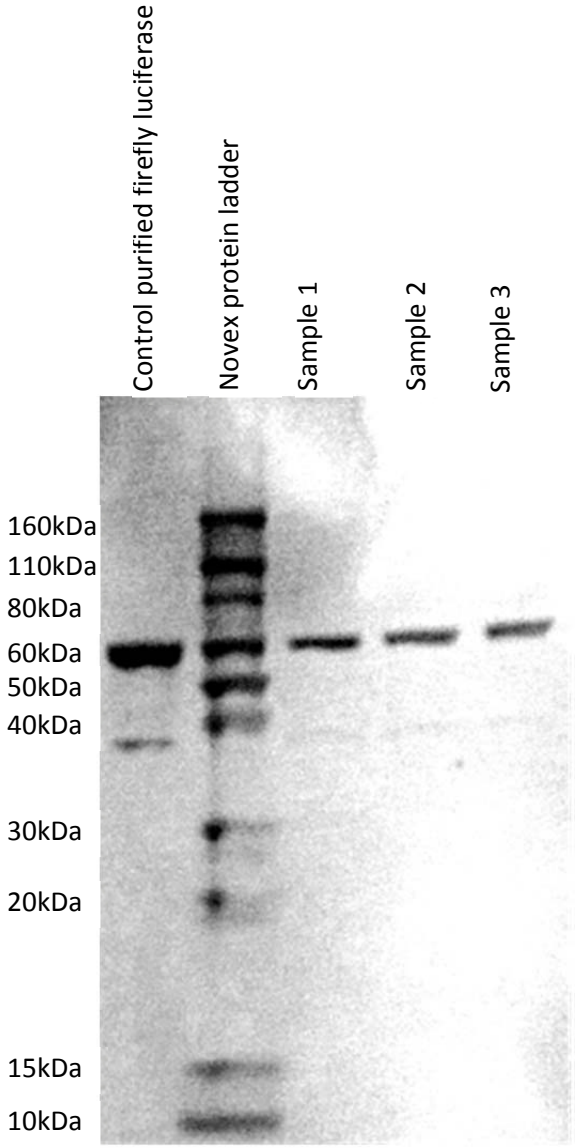

Fig. S4. Western blot analysis of firefly luciferase expression. Protein chromatography was performed using Novex™ 14% Tris-Glycine Mini Protein Gels; primary antibody staining was performed with mouse monoclonal Anti-6X His tag antibodies (Abcam); and secondary staining was performed using WesternBreeze Chromogenic Kit, anti-mouse (Thermo Scientific). **Sample 1**: Firefly luciferase expression under T7 promoter in a bacterial TX/TL system. **Sample 2**: Firefly luciferase expression under

the Tet promoter in a bacterial TX/TL system. **Sample 3**: Luciferase expression in a HeLa TX/TL system after transcription using HeLa nuclear extract. The sample used in this experiment is the same as in the 1:1 A:B ratio in **Fig. 6f**. Prior to loading of the gel, luciferase activity in aliquots of each sample was measured, and the obtained luminescence signal was used to approximately normalize the concentration (loading volume) of all samples. As a positive control, purified full-length recombinant firefly luciferase protein (Abcam) was used.

Fig. S5

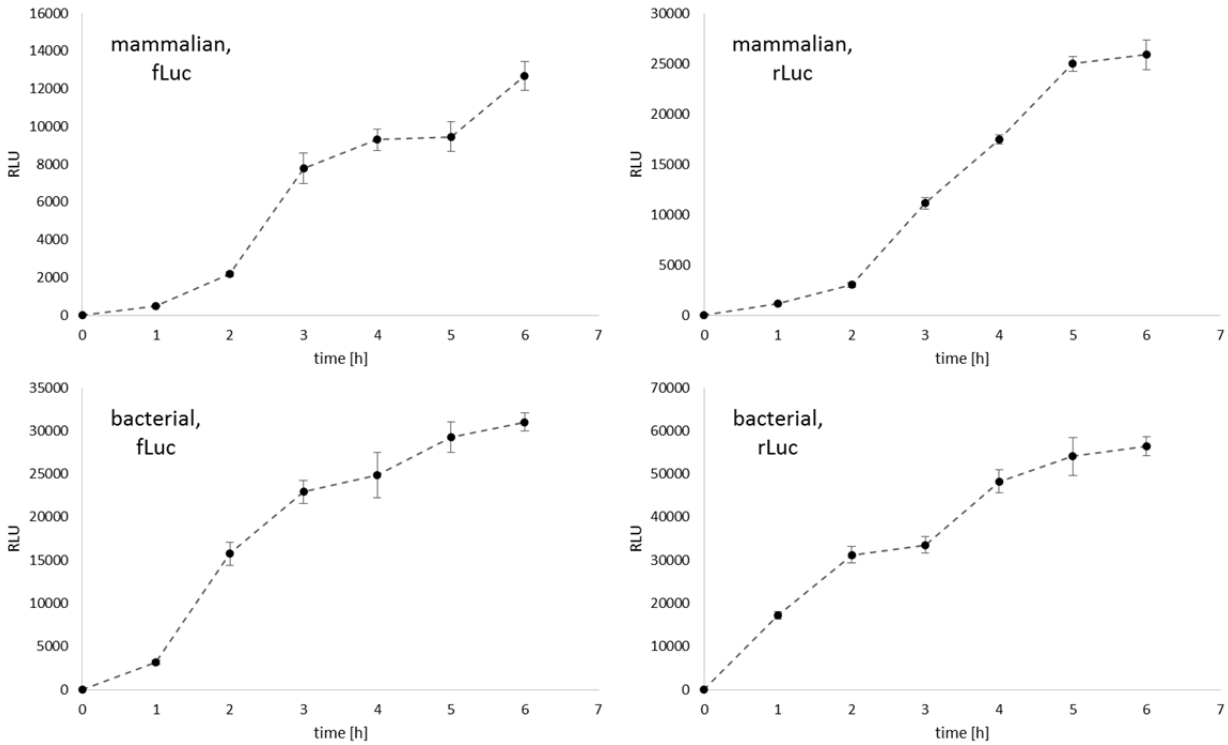

Fig. S5. Comparison of bacterial and mammalian TX/TL, for firefly and Renilla luciferases (fLuc and rLuc). Dotted lines are visual guides, not data fits. Error bars indicate S. E. M., n=4.

Fig. S6

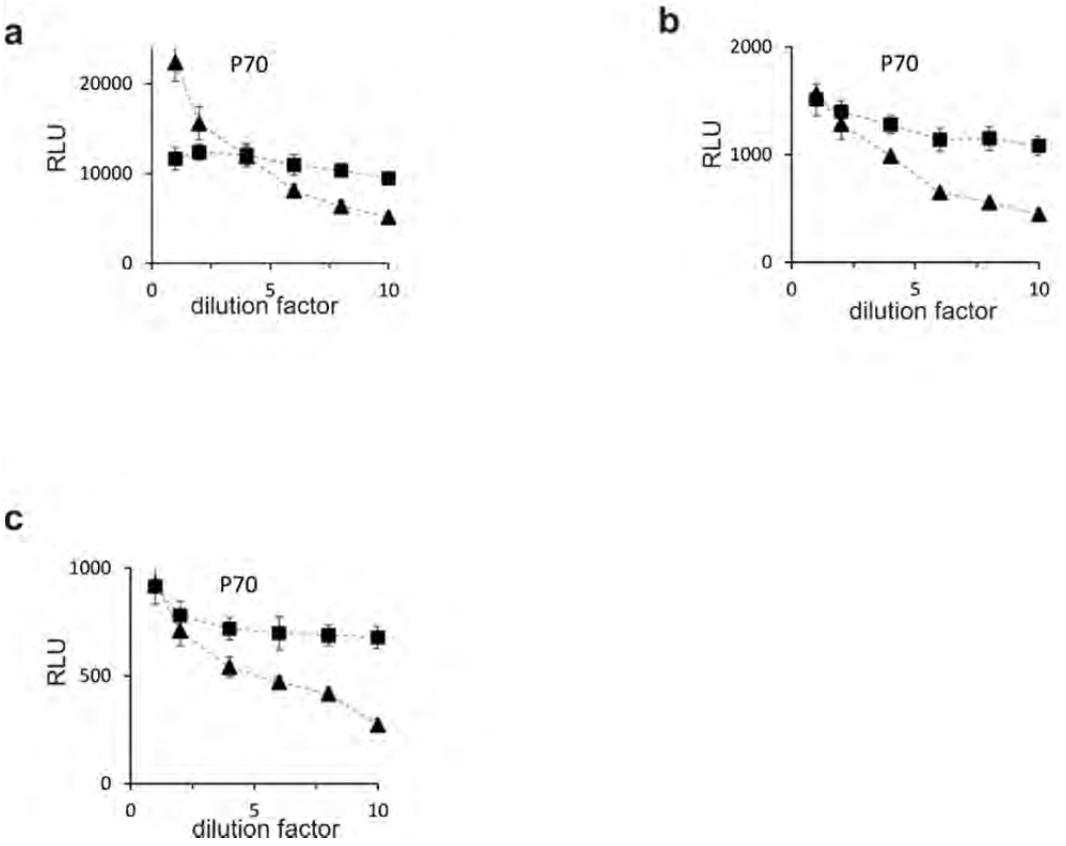

Fig. S6. Effects of dilution on fLuc expression in liposomes and unencapsulated reactions. Expression of one-, two-, and three-peptide systems under control of the P70 promoter, without small molecule activation. **a.** One-part luciferase system (as in **Fig. 3d**). **b.** Two-part split luciferase system (as in **Fig. 3e**). **c.** Three-part scaffolded split luciferase system (as in **Fig. 3f**).

Fig. S7

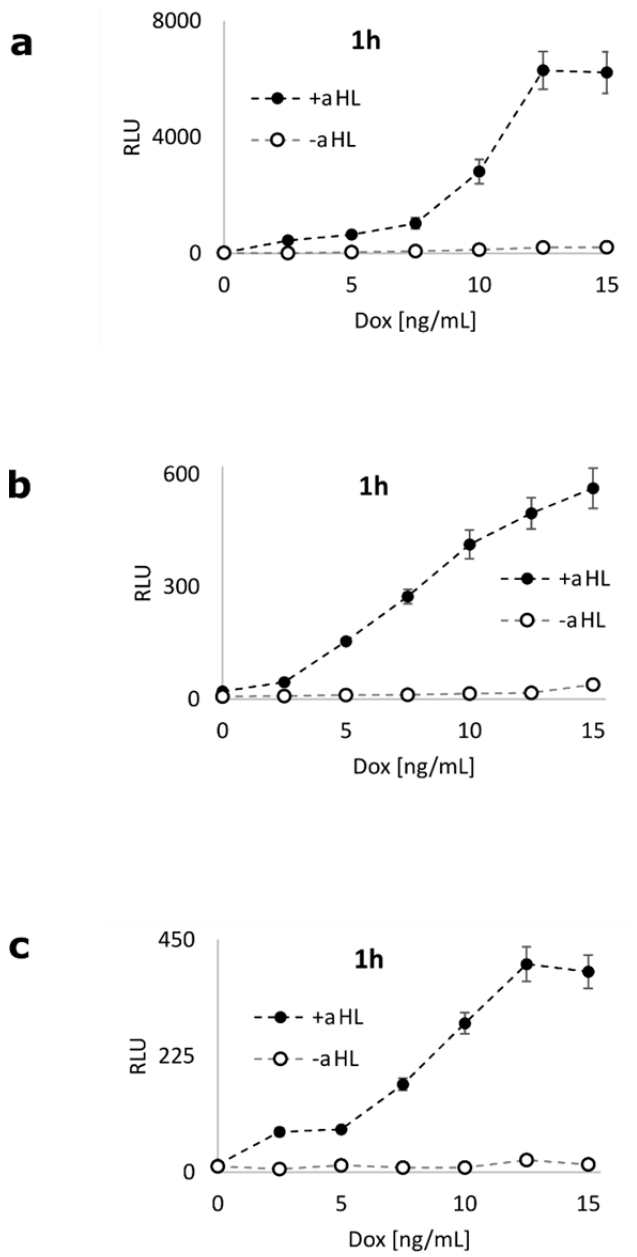

Fig. S7. End-point expression of luciferase from each of the expression systems presented in **Fig. 3**, measured at end point 1 h, at 7 different concentrations of Dox. The dotted lines are visual guides, not fits. **a.** One-part luciferase system (as in **Fig. 3g**). **b.** Two-part split luciferase system (as in **Fig. 3h**). **c.** Three-part scaffolded split luciferase system (as in **Fig. 3i**).

Fig. S8

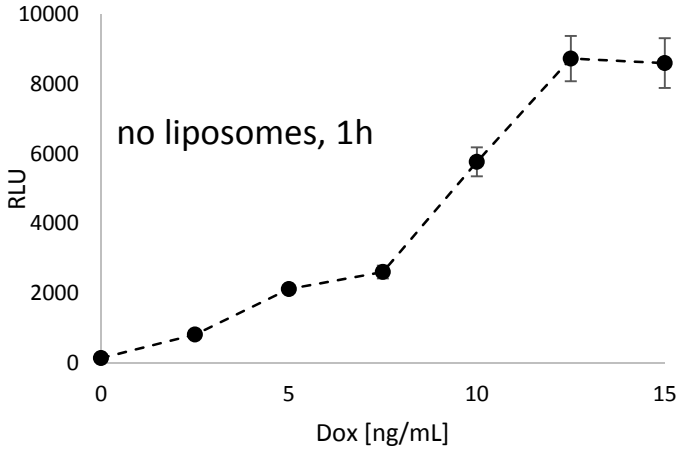

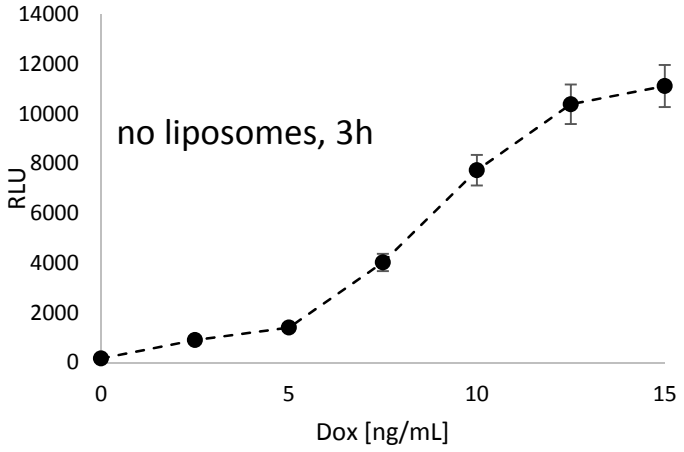

Fig. S8: Single-protein fLuc expression in solution (as in **Fig. 3g**), 5 nM plasmid.

Fig. S9

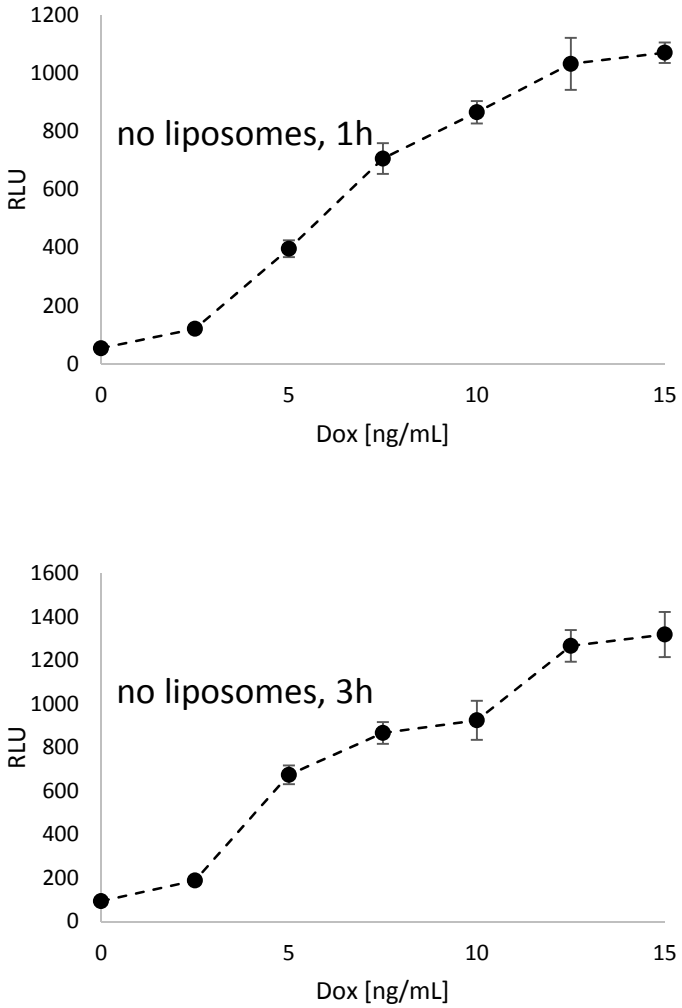

Fig. S9: Two-protein fLuc expression in solution, plasmids for fLucA and fLucB combined at 2.5 nM each (as in **Fig. 3h**).

Fig. S10

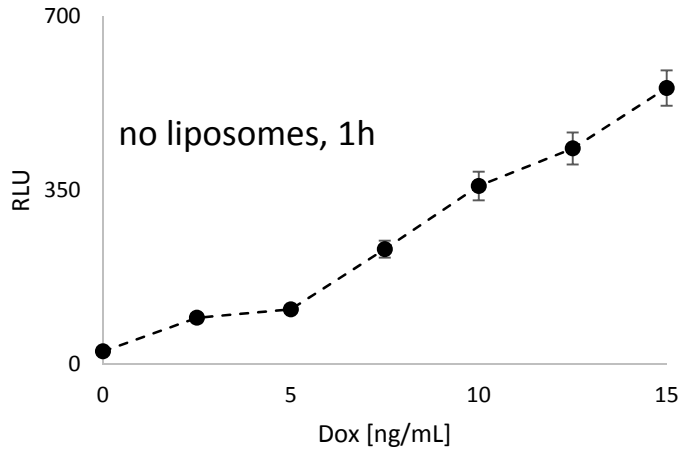

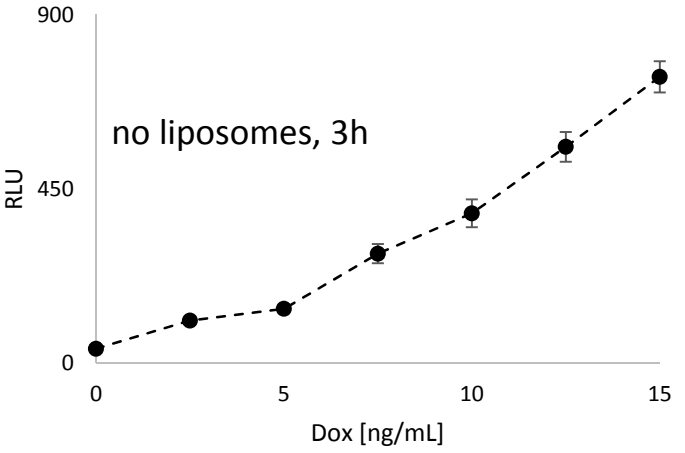

Fig. S10: Three-protein fLuc expression in solution; plasmids fLucC, fLucD, and Scaffold combined at 1.67 nM each (as in **Fig. 3i**).

Fig. S11

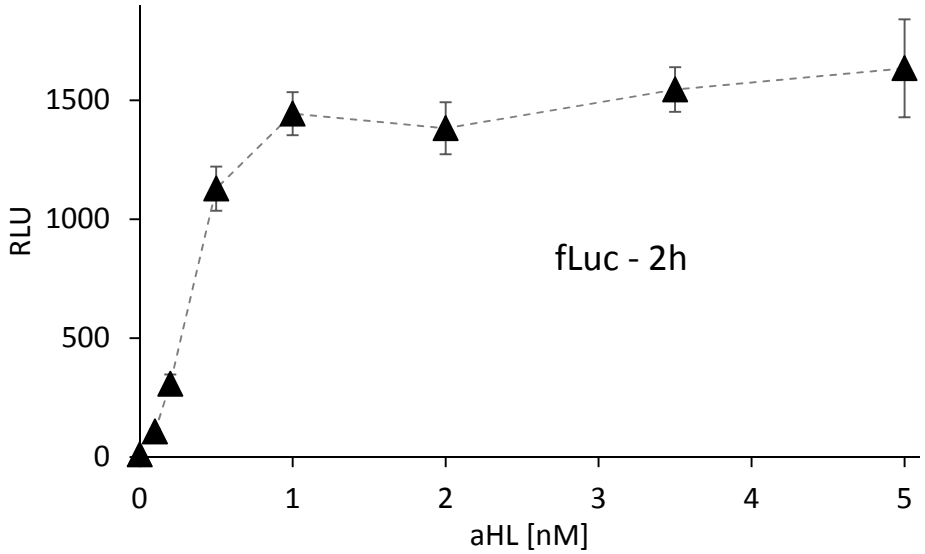

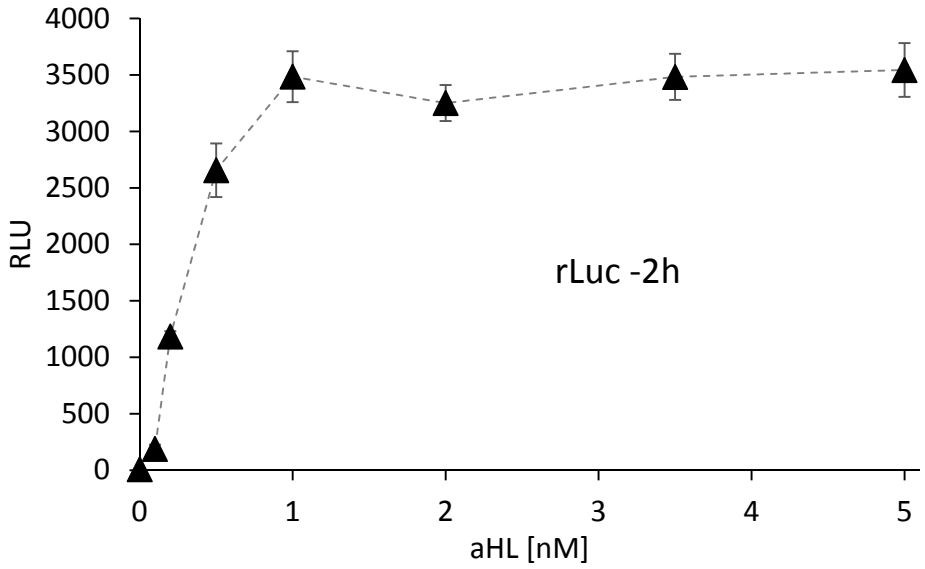

Fig. S11: Expression of fLuc and rLuc at 2 h end-point, from liposomes with different concentration of aHL plasmid (as in **Fig. 4**).

Fig. S12

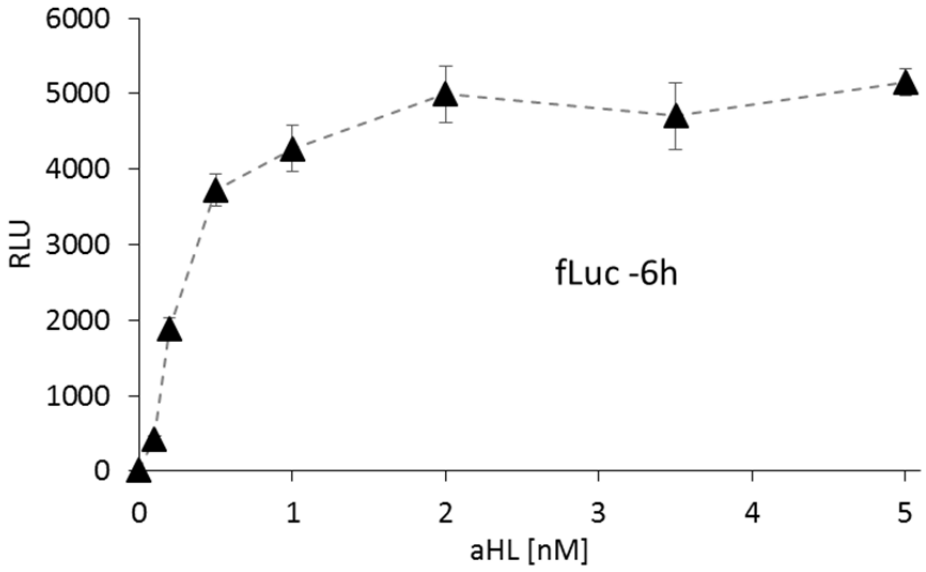

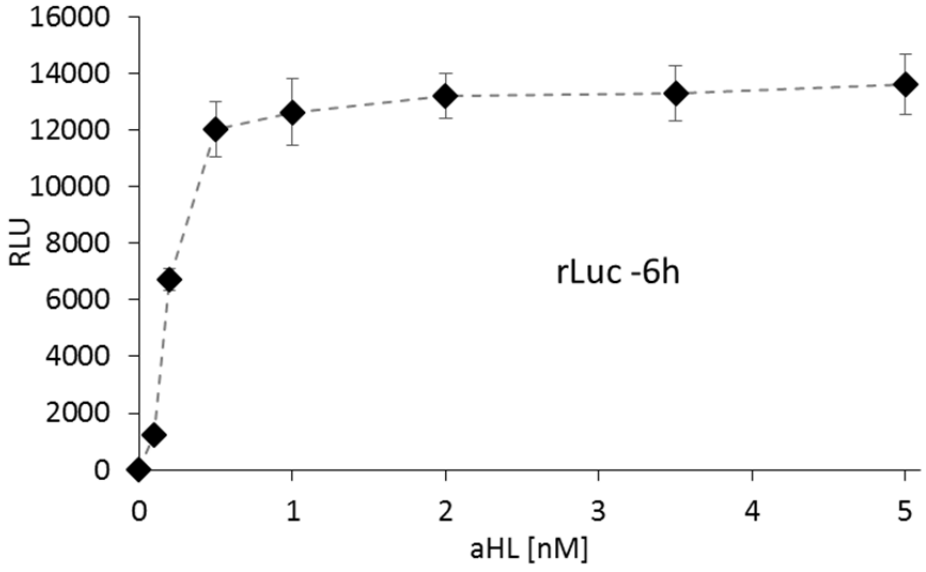

Fig. S12: Expression of fLuc and rLuc at 6 h end-point, from liposomes with different concentration of aHL plasmid (as in **Fig. 4**).

Fig. S13

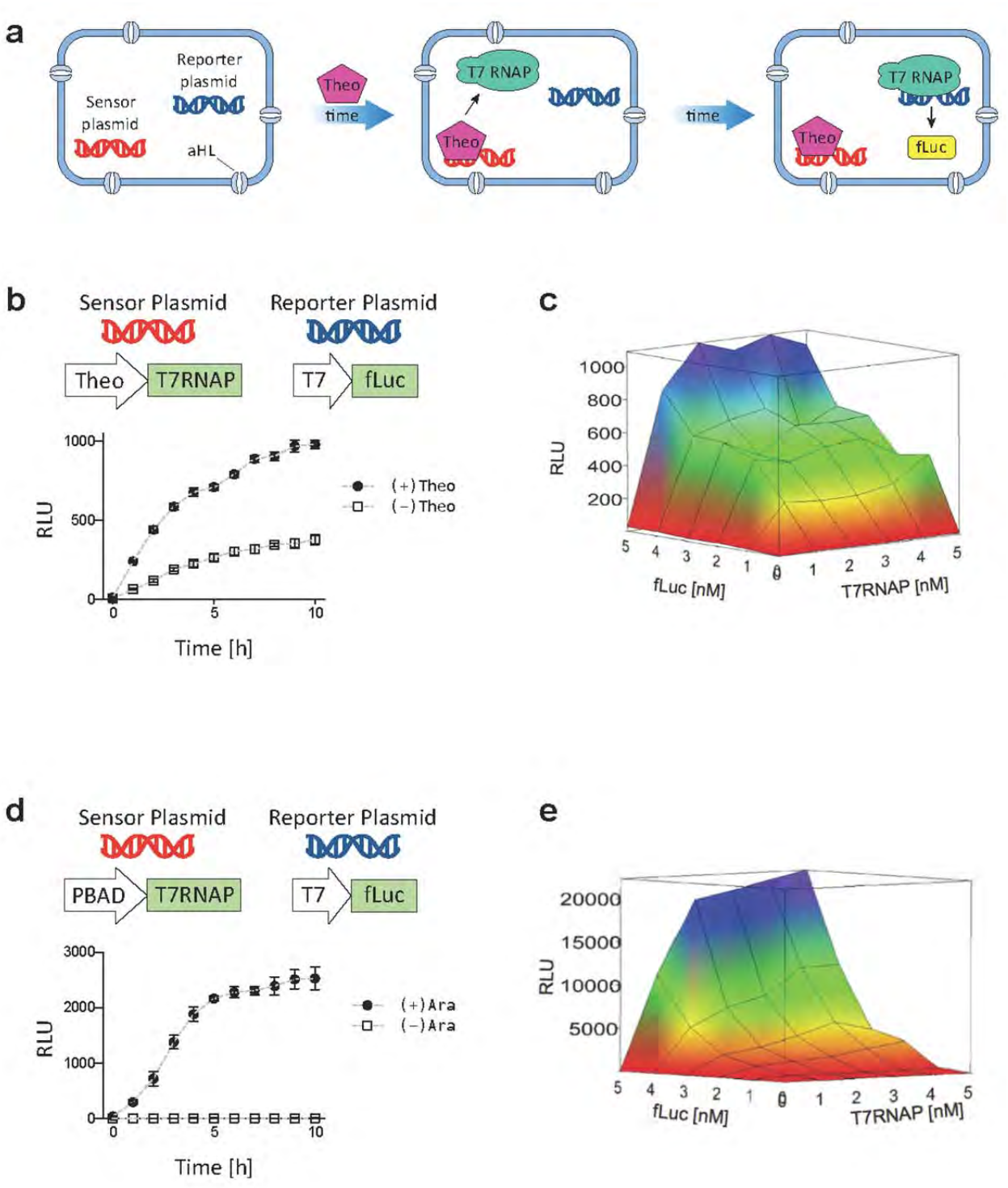

Fig. S13. Activation of liposomally encapsulated cascaded genetic networks via membrane-permeable small molecules. a. Schematic of synthetic minimal cells created. The liposomes used in this figure were built with bacterial transcription/translation (TX/TL) components; they contain the gene for T7 RNA Polymerase (T7RNAP) under an inducible element—either the Theo aptamer, which responds to theophylline (Theo), or the PBAD promoter, which responds to arabinose (Ara)—and the gene for firefly luciferase (fLuc) under a T7 promoter. A small molecule activator (Theo or Ara) drives T7RNAP expression, which in turn drives fLuc expression. **b-c.** The theophylline-triggered genetic cascade. **b.** fLuc expression over time, with and without 2 mM Theo; each of the two plasmids is present at 5 nM. **c.** Final fLuc expression at different concentrations of each plasmid, all measured after 10 h of expression. **d-e.** The arabinose-triggered genetic cascade. **d.** fLuc expression over time, with and without 10 mM Ara; each of the two plasmids is present at 5 nM. **e.** Final fLuc expression at different concentration of each plasmid, all measured after 10 h of expression. All data points are an average of 4 replicates; error bars indicate S. E. M.

Fig. S14

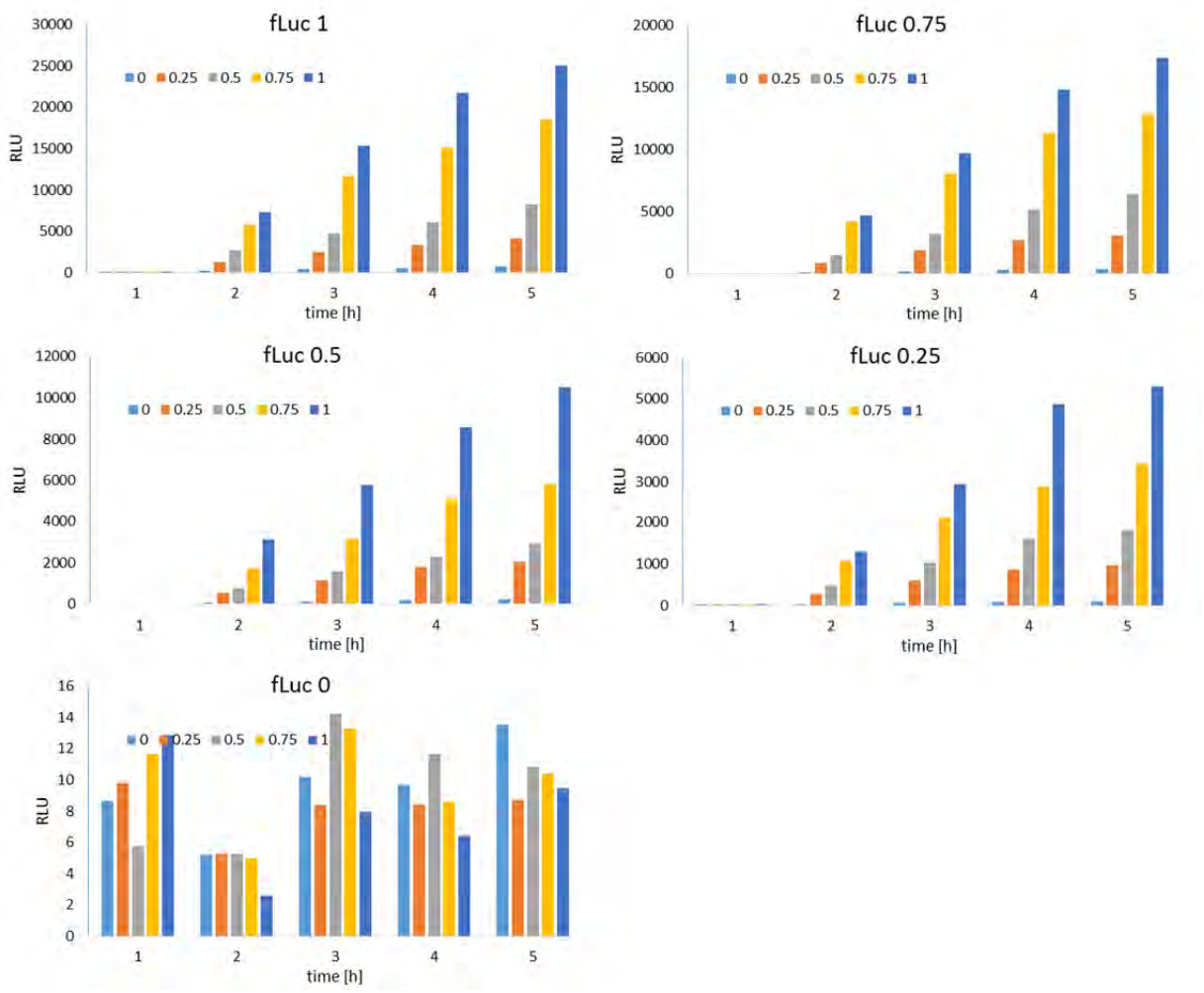

Fig. S14: Time-course of expression of fLuc under the lac promoter, with different ratios of liposomes (as in **Fig. 5c**). Occupancies are numerically defined as in the legend for **Fig. 5**.

Fig. S15

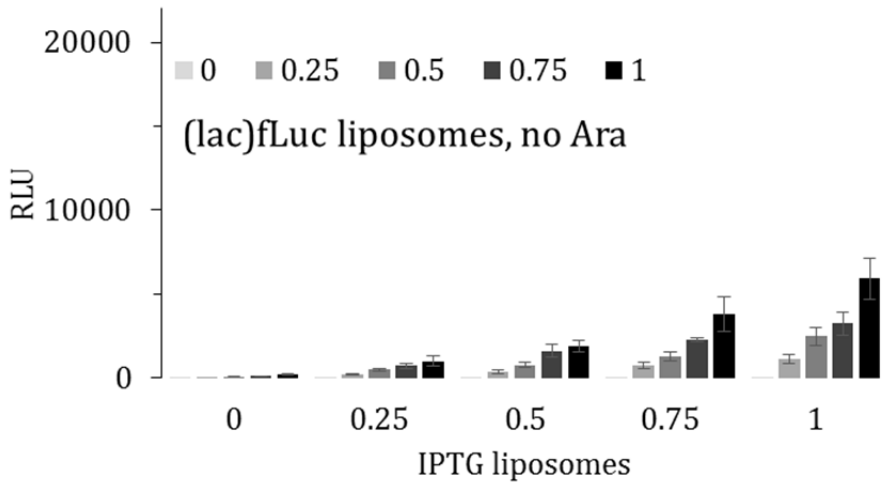

Fig. S15. Expression of fLuc under lac promoter in absence of arabinose (as in **Fig. 5c**). Occupancies are numerically defined as in the legend for **Fig. 5**.

Fig. S16

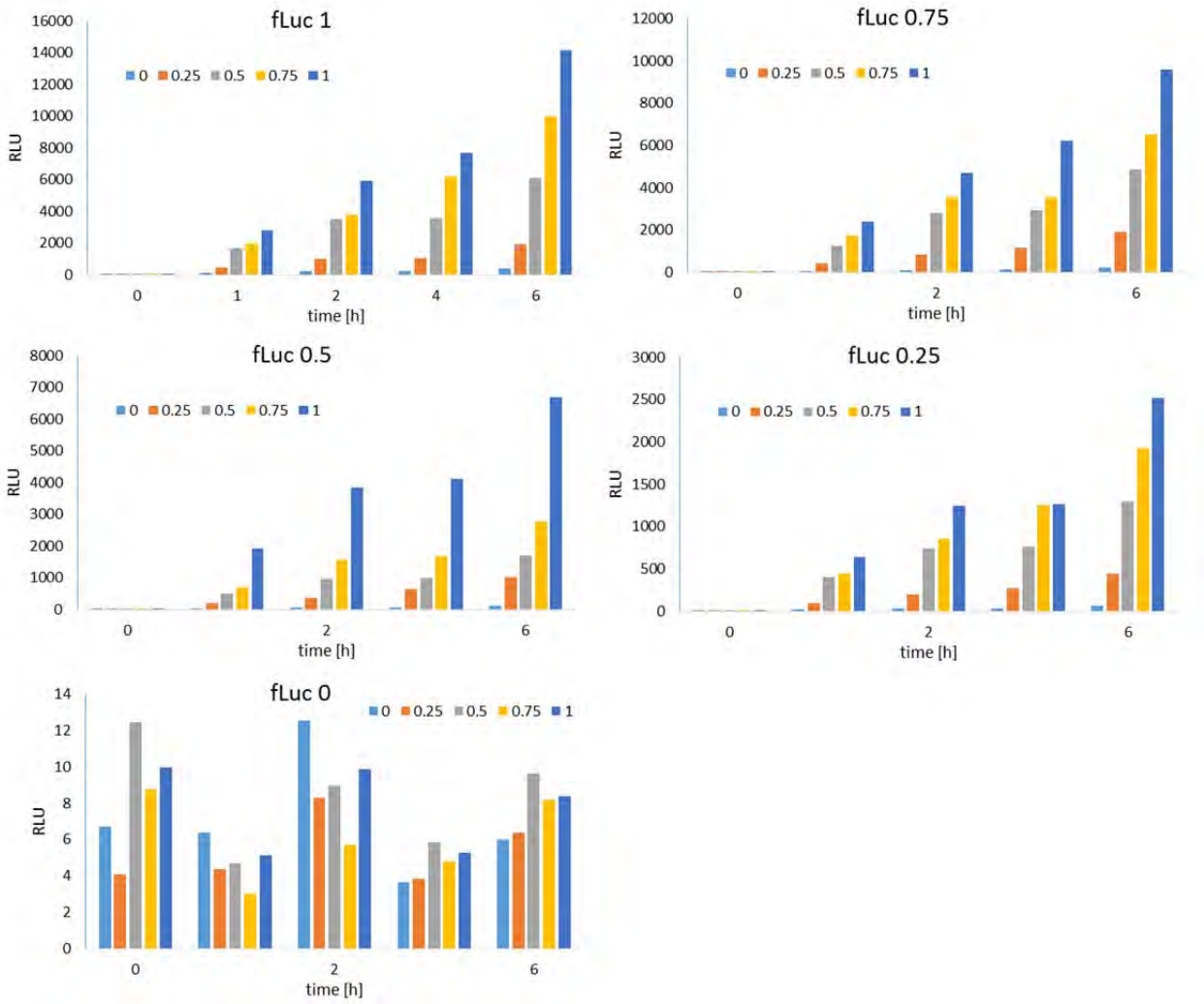

Fig. S16: Time course of fLuc under T7 promoter, driven by T7RNAP under the lac promoter, with different ratios of liposomes (as in **Fig. 5d**). Occupancies are numerically defined as in the legend for **Fig. 5**.

Fig. S17

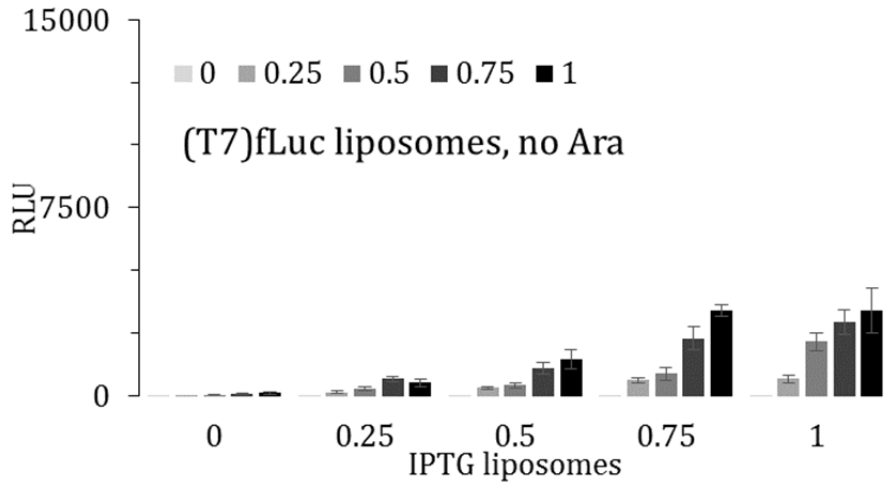

Fig. S17. Expression of fLuc under the T7 promoter, driven by T7RNAP under the lac promoter, in the absence of Arabinose (as in **Fig. 5d**). Occupancies are numerically defined as in the legend for **Fig. 5**.

Fig. S18

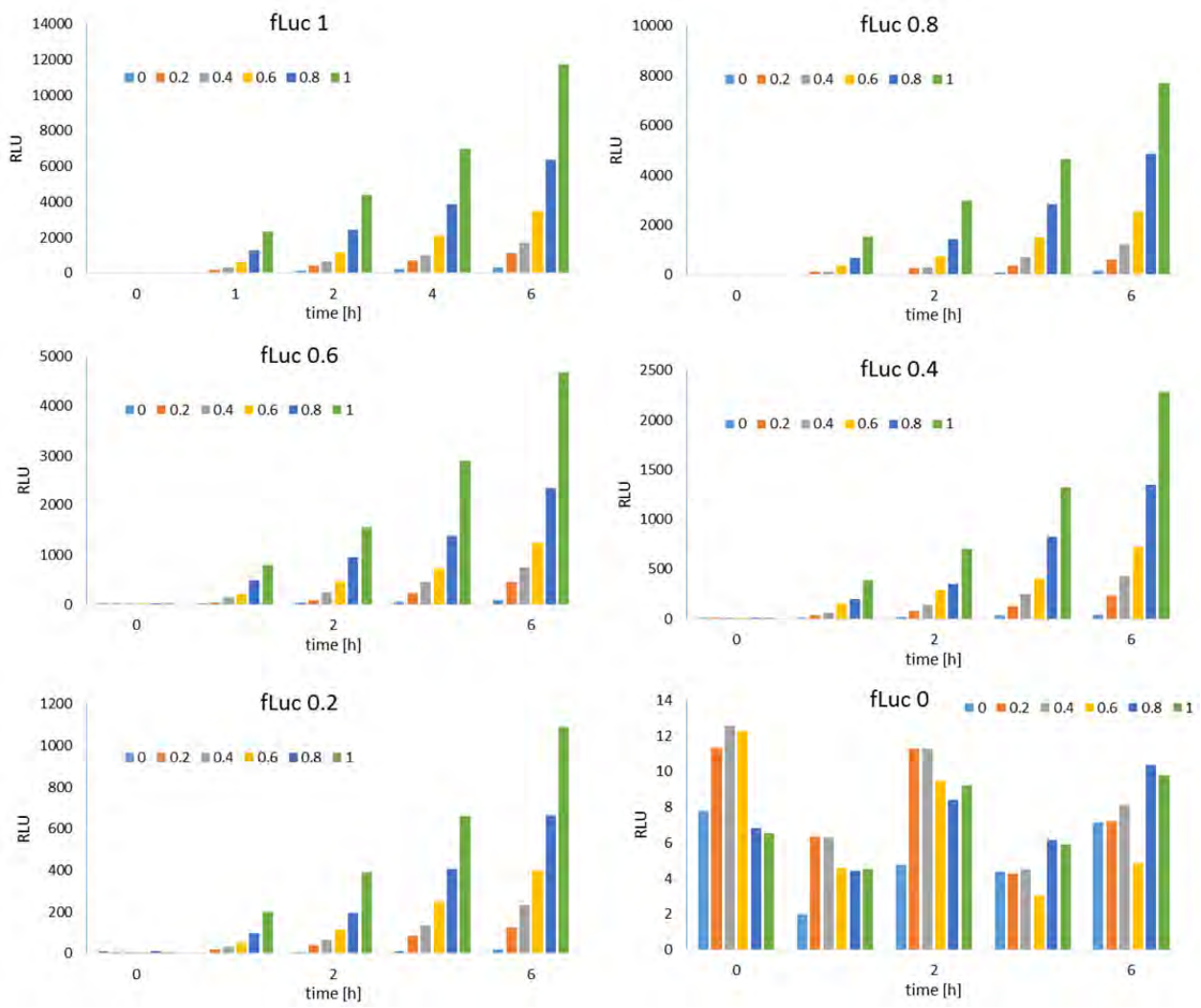

Fig. S18. Time course of fLuc expression at different ratios of fLuc and Tet liposomes (as in **Fig. 5f**). Occupancies are numerically defined as in the legend for **Fig. 5**.

Fig. S19

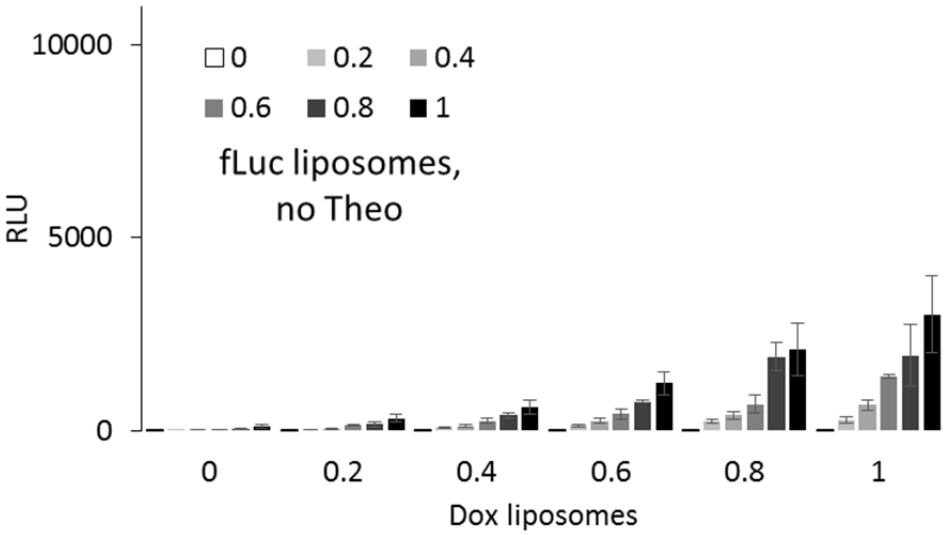

Fig. S19: End-point data for fLuc expression without theophylline (as in **Fig. 5f**). Occupancies are numerically defined as in the legend for **Fig. 5**.

Fig. S20

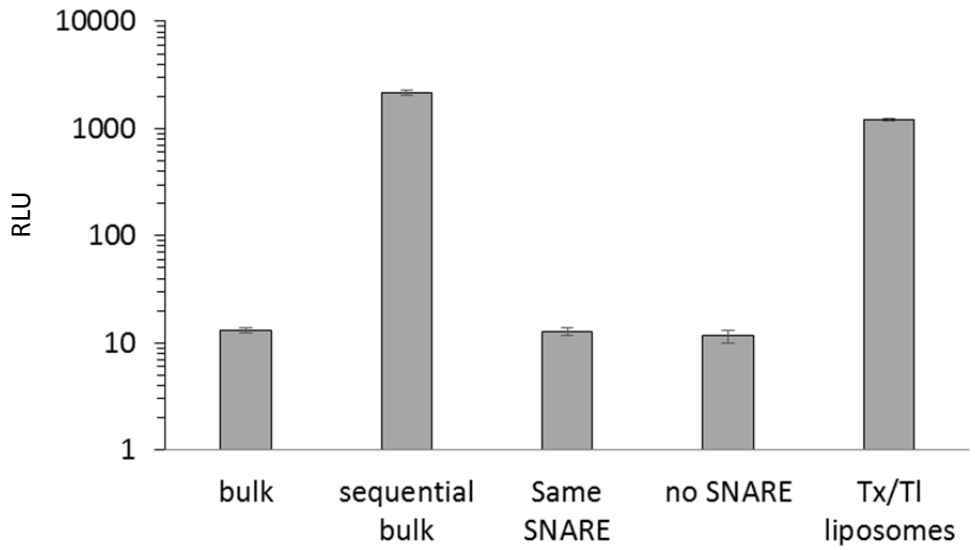

Fig. S20. Cell-free transcription and translation in mammalian cell-free systems. From left to right, the bars correspond to:

Bulk: cell-free TX and TL systems, same as used in experiments presented in **Fig. 6f**, but mixed in one tube instead of encapsulating in separate liposomes, and incubated for 24 hours at 37°C.

Sequential bulk: the TX reaction incubated for 12 hours, then mixed with equal volume of the TL mixture, incubated for another 12 hours (like experiment of **Fig. 6f**, but without liposome encapsulation).

Same SNARE, no SNARE and TX/TL liposomes are the same data as presented on **Fig. 6f**, shown here again for reference.

Fig. S21

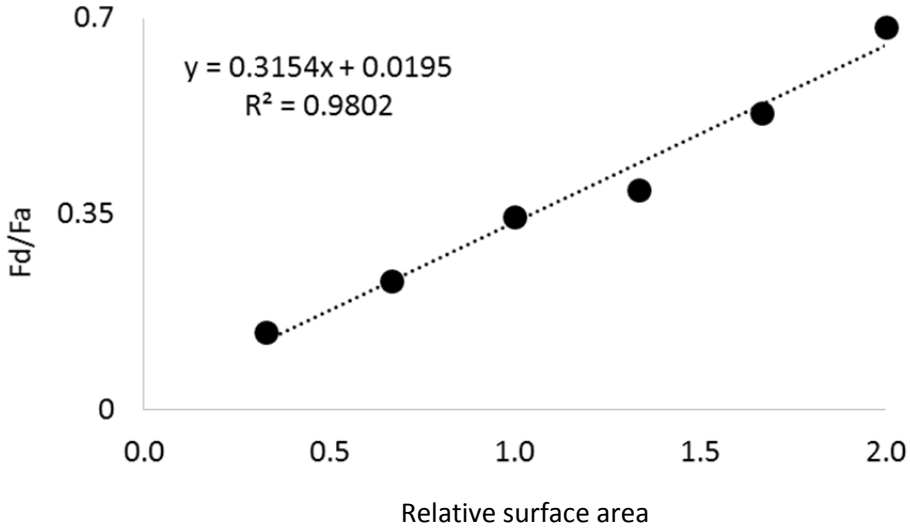

Fig. S21. Calibration curve for FRET response. The samples were prepared with varying ratios of the FRET dye pair lipids (Lissamine™ Rhodamine B 1,2-Dihexadecanoyl-sn-Glycero-3-Phosphoethanolamine, Triethylammonium Salt and NBD-PE (N-(7 Nitrobenz-2-Oxa-1,3-Diazol-4-yl)-1,2-Dihexadecanoyl-sn-Glycero-3-Phosphoethanolamine, Triethylammonium Salt)) to the POPC:cholesterol lipid mix, in order to mimic surface area change in fusion experiments. Fd, fluorescence of donor; Fa, fluorescence of acceptor; the relative surface area of 1 is defined as the starting ratio of FRET dyes to lipids in the SNARE fusion experiment samples, and subsequent values of surface are obtained by scaling proportionally (increasing or decreasing) the concentration of FRET dyes in the membrane, as described previously.[36,37]

Fig. S22

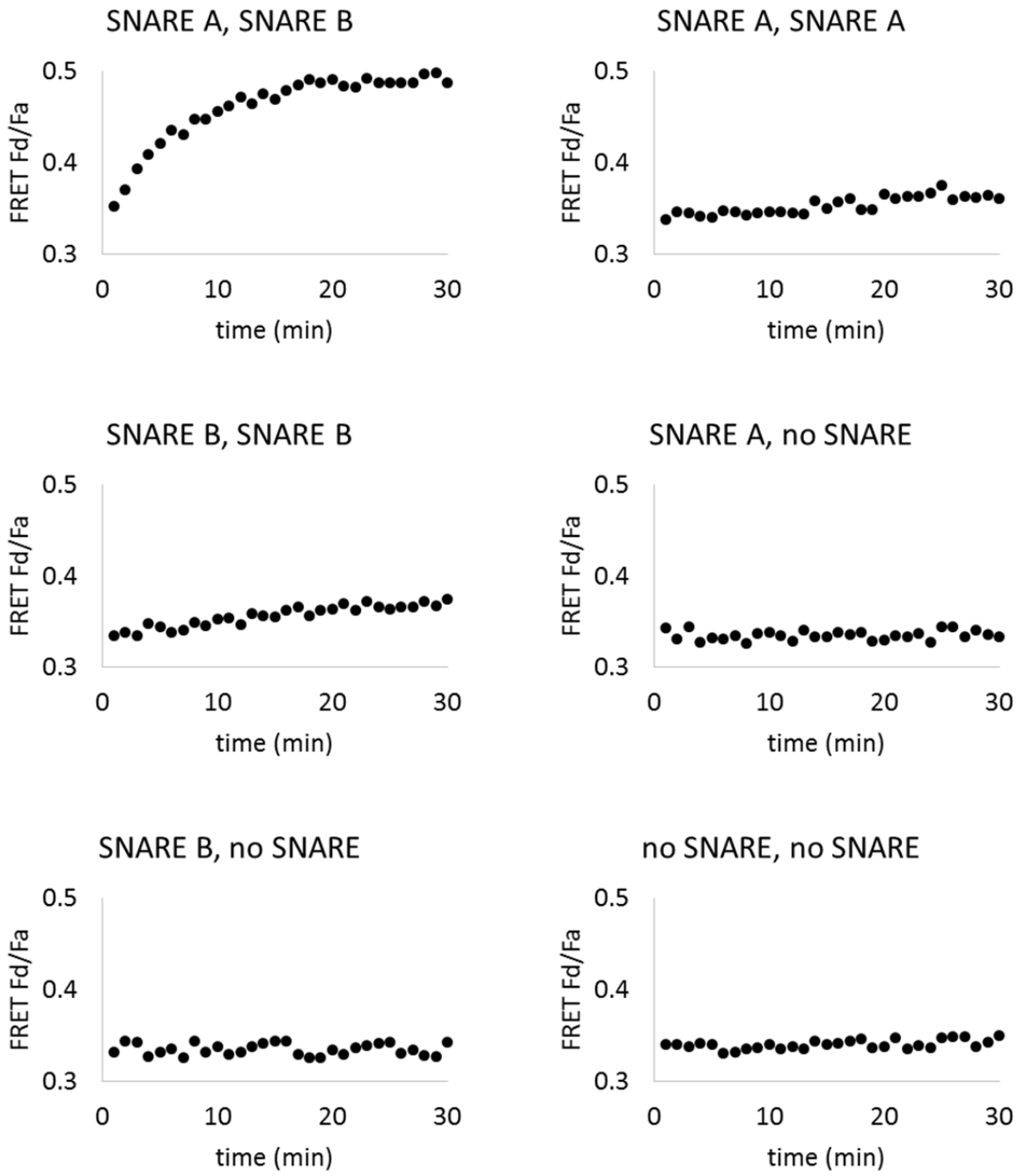

Fig. S22. Liposome fusion induced by SNARE protein mimics. The mixing of liposomes was measured with changes of FRET signal from the FRET donor and acceptor dyes in the liposomes, both to confirm mixing and as a way to estimate the time course of vesicle size increases due to fusion. For experimental details, see **Materials and Methods**. The letters A and B represent a pair of SNAREs that bind to one another; when A is paired with A, or B with B, no binding or fusion happens.

Fig. S23

sample	**1**	**2**	**3**	**4**	**5**	**6**
probe	SNARE A	SNARE B	SNARE A	SNARE A	SNARE B	SNARE B
positive target	SNARE B	SNARE A	SNARE A	no SNARE	SNARE B	no SNARE
sample	**7**	**8**	**9**	**10**	**11**	**12**
probe	SNARE A	SNARE B	SNARE A	SNARE A	SNARE B	SNARE B
negative target	SNARE B	SNARE A	SNARE A	no SNARE	SNARE B	no SNARE

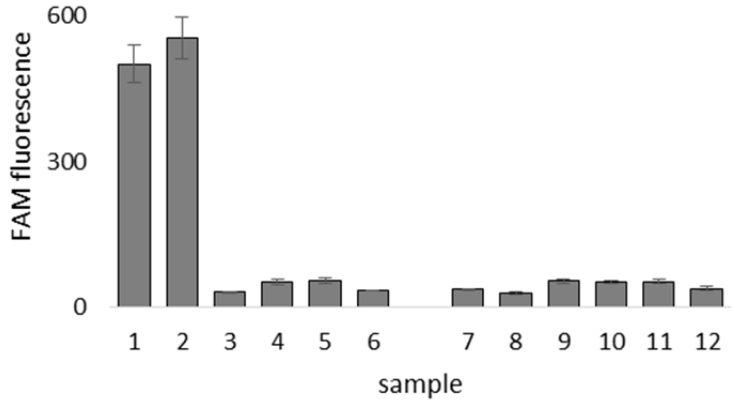

Fig. S23. De-quenching of a liposome-encapsulated molecular beacon upon SNARE mediated fusion with liposomes encapsulating a complementary target. Molecular beacon FAM-5'-GCGAGCTAGGAAACACCAAAGATGATATTTGCTCGC -3'-DABCYL was encapsulated in one population of liposomes ("probe" liposomes), and a complementary target ("positive target") or a non-complementary target ("negative target") were encapsulated in the other population of liposomes. Liposomes were prepared and purified according to the general procedures described in **Material and Methods**. Samples were then mixed, incubated for 30 min at room temperature, and fluorescence of the fluorescein (FAM) dye was measured. The increased fluorescence indicates de-quenched FAM probe as a result of hybridization of a molecular beacon to the target sequence, and thus mixing of the content of the liposomes upon SNARE-mediated fusion. Error bars indicate S.E.M. n=3.

Fig. S24

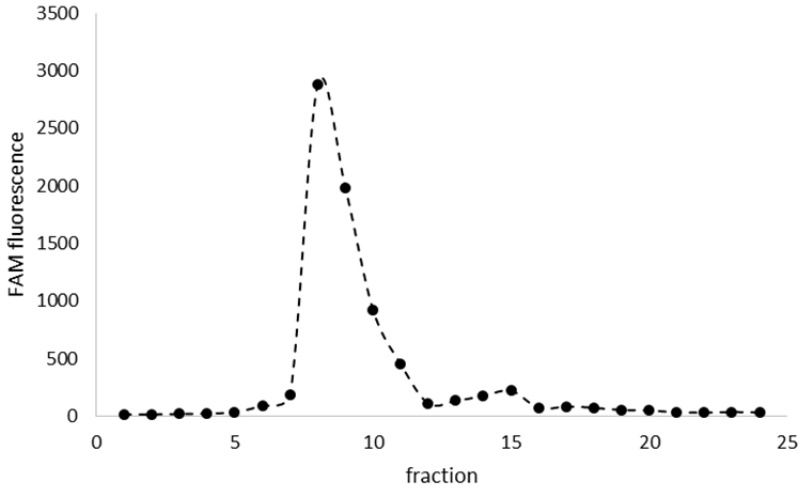

Fig. S24. Leakage of DNA oligonucleotide from liposomes after SNARE-induced fusion. The fluorescent oligonucleotide 5'-FAM-d(GCG CAT TGG)-3' was encapsulated at 1 µM in both populations of liposomes containing SNARE A and SNARE B (a matched pair, as defined in **Fig. 6a**). The liposomes were extruded and purified as described in **Materials and Methods**, and fusion reactions were performed. After fusion and 1 h equilibration, the sample was purified on a Sepharose 4B size-exclusion column. The combined total free-molecule fraction fluorescence is about 8.2% of the total fluorescence measured from all liposome and free-molecule fractions (we defined the liposome fraction as the sum of fractions 6 to 12, and the free-molecule fraction as the sum of fractions 13 to 17).

Fig. S25

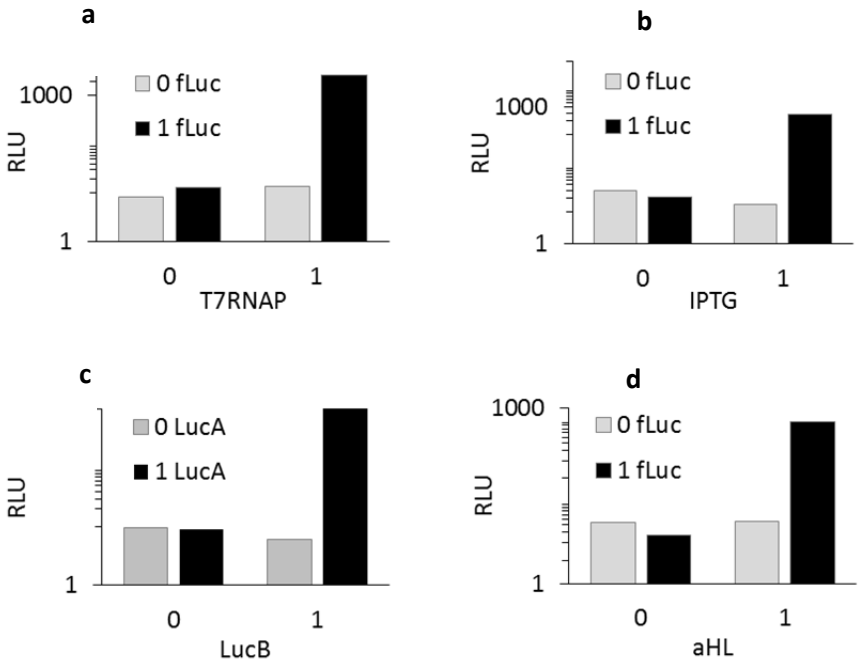

Fig. S25: Fusion of liposomes and subsequent merging of independent genetic circuits using SNARE protein mimics—with liposome pairs reversed compared to the experiments shown in **Fig. 6**. These experiments were designed analogously to the results presented in **Fig. 6**: two populations of liposomes were prepared, each with one of the SNARE protein mimics (see **Fig. 6a** for the experimental setup). Equal volumes of each population were mixed, containing two different concentrations of the liposomes: 10 mM (1) or zero (0), resulting in 4 different ratios of liposomes tested. All samples were incubated for 6 h after mixing, after which end-point fLuc luminescence was analyzed as described in **Materials and Methods**. **a.** Cascading genetic circuit of **Fig. 6b** with flipped SNAREs: T7RNAP under the P70 promoter (SNARE_B) mixed with fLuc under T7 promoter (SNARE_A). **b.** Delivering small molecule activator: fLuc under lac promoter (SNARE_B) mixed with IPTG-filled liposomes (SNARE_A), as in **Fig. 6c** but with flipped SNAREs. **c.** Creating protein reconstitution system: fLucA (SNARE_B) mixed with fLucB (SNARE_A), as in **Fig. 6e** but with flipped SNAREs. **d.** Enabling small molecule activation: liposomes expressing aHL (SNARE_B) mixed with fLuc under lac promoter (SNARE_A), IPTG added to the external solution, as in **Fig. 6d** but with SNAREs flipped.

Fig. S26

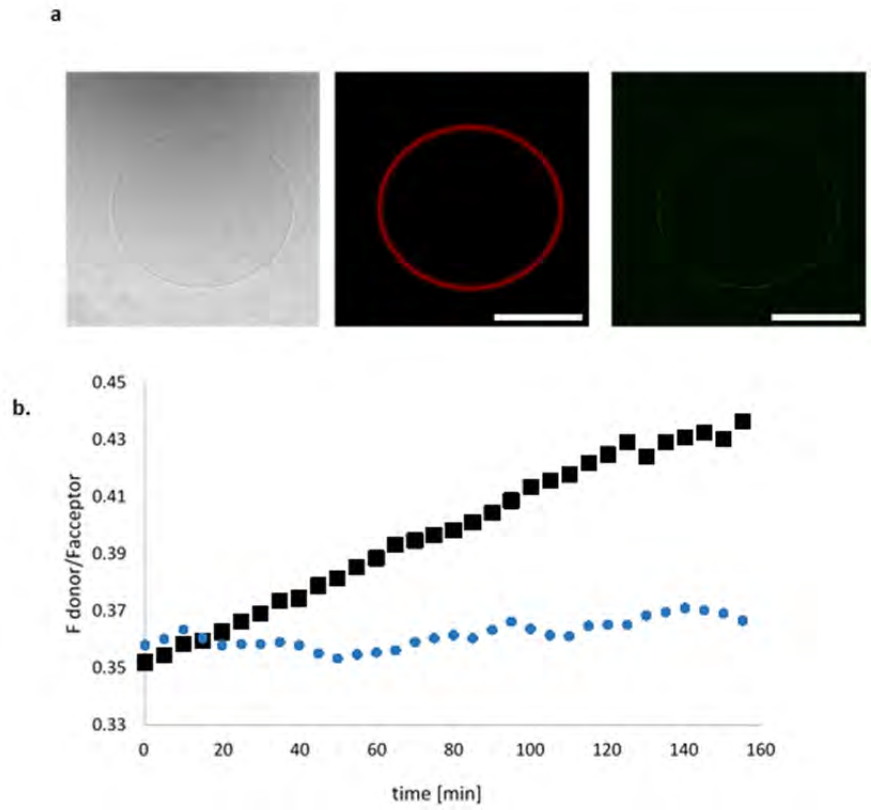

Fig. S26: Incorporation of alpha hemolysin protein into phospholipid bilayer membrane. **a** Confocal microscopy images of liposome expressing alpha hemolysin—mClover protein fusion, with liposome membrane labeled with red dye (rhodamine functionalized with a lipid tail, Lissamine rhodamine B). Giant unilamellar vesicles were prepared according to previously described methods[19], and non-encapsulated TL/TL mixture was removed by dialysis as described in **Materials and Methods.** The scale bar is 5µm. **b**. Incorporation of alpha hemolysin protein in the bilayer membrane of the phospholipid liposome is measured by FRET (Fluorescence Resonance Energy Transfer). The membrane is labeled with two FRET pair dyes: Lissamine Rhodamine B 1,2-Dihexadecanoyl-sn-Glycero-3-Phosphoethanolamine, Triethylammonium Salt and NBD-PE N-(7 Nitrobenz-2-Oxa-1,3-Diazol-4-yl)-1,2-Dihexadecanoyl-sn-Glycero-3-Phosphoethanolamine, Triethylammonium Salt. The alpha hemolysin was constituently expressed inside liposomes using a bacterial TX/TL system and the bacterial P70 promoter (black squares); as a control a soluble, non-membrane associated protein (firefly luciferase) was expressed under the same conditions (blue circles).

Supplementary Tables

Abbreviations

Common abbreviations used throughout the **Supplementary Tables**:

Abbreviation	Meaning
Diff.	Difference
ns	Not significant
CI	Confidence interval
Nparm	Number of parameters
DF	Degrees of freedom
*	Significant
****	More significant

Table S1

Statistics for **Fig. 3d**: 2-way ANOVA with factors of "Dilution Factor" and "Encapsulation".

Source of Variation	% of total variation	P value	P value summary	Significant?
Interaction	29.8	< 0.0001	****	Yes
Dilution Factor	57.94	< 0.0001	****	Yes
Encapsulation	3.859	0.0002	***	Yes

Dunnett's multiple comparisons test after the ANOVA.

	Mean Diff.	95% CI of diff.	Significant?	Summary	Adjusted P Value
Liposome					
2 vs. 1	-500.6	-1552 to 551.2	No	ns	0.6003
4 vs. 1	-496	-1548 to 555.9	No	ns	0.6084
6 vs. 1	-1005	-2057 to 46.55	No	ns	0.0652
8 vs. 1	-1106	-2158 to -54.09	Yes	*	0.0364
10 vs. 1	-913.1	-1965 to 138.7	No	ns	0.1071
Solution					
2 vs. 1	-2631	-3683 to -1579	Yes	****	< 0.0001
4 vs. 1	-3916	-4968 to -2865	Yes	****	< 0.0001
6 vs. 1	-5429	-6481 to -4378	Yes	****	< 0.0001
8 vs. 1	-5917	-6969 to -4866	Yes	****	< 0.0001
10 vs. 1	-6358	-7409 to -5306	Yes	****	< 0.0001

Table S2

Statistics for **Fig. 3e**: 2-way ANOVA with factors of "Dilution Factor" and "Encapsulation".

Source of Variation	% of total variation	P value	P value summary	Significant?
Interaction	38.48	< 0.0001	****	Yes
Dilution Factor	50.55	< 0.0001	****	Yes
Encapsulation	1.665	0.0156	*	Yes

Dunnett's multiple comparisons test after the ANOVA.

	Mean Diff.	95% CI of diff.	Significant?	Summary	Adjusted P Value
Liposome					
2 vs. 1	-27.26	-177.3 to 122.8	No	ns	0.9854
4 vs. 1	-42.54	-192.6 to 107.5	No	ns	0.9129
6 vs. 1	-26.02	-176.1 to 124.1	No	ns	0.9881
8 vs. 1	-29.94	-180.0 to 120.1	No	ns	0.9781
10 vs. 1	-97.95	-248.0 to 52.13	No	ns	0.31
Solution					
2 vs. 1	-385.3	-535.4 to -235.2	Yes	****	< 0.0001
4 vs. 1	-582.8	-732.9 to -432.8	Yes	****	< 0.0001
6 vs. 1	-753.1	-903.2 to -603.0	Yes	****	< 0.0001
8 vs. 1	-827.7	-977.7 to -677.6	Yes	****	< 0.0001
10 vs. 1	-878.8	-1029 to -728.7	Yes	****	< 0.0001

Table S3

Statistics for **Fig. 3f**: 2-way ANOVA with factors of "Dilution Factor" and "Encapsulation".

Source of Variation	% of total variation	P value	P value summary	Significant?
Interaction	25.06	< 0.0001	****	Yes
Dilution Factor	34.95	< 0.0001	****	Yes
Encapsulation	33.06	< 0.0001	****	Yes

Dunnett's multiple comparisons test after the ANOVA.

	Mean Diff.	95% CI of diff.	Significant?	Summary	Adjusted P Value
Liposome					
2 vs. 1	15.96	-54.75 to 86.66	No	ns	0.9637
4 vs. 1	0.3899	-70.32 to 71.10	No	ns	> 0.9999
6 vs. 1	-14.33	-85.03 to 56.38	No	ns	0.9767
8 vs. 1	-22.41	-93.11 to 48.30	No	ns	0.8716
10 vs. 1	-44.25	-115.0 to 26.45	No	ns	0.3474
Solution					
2 vs. 1	-228.6	-299.3 to -157.9	Yes	****	< 0.0001
4 vs. 1	-314.7	-385.4 to -244.0	Yes	****	< 0.0001
6 vs. 1	-345.7	-416.4 to -275.0	Yes	****	< 0.0001
8 vs. 1	-382.9	-453.6 to -312.2	Yes	****	< 0.0001
10 vs. 1	-394.8	-465.5 to -324.0	Yes	****	< 0.0001

Table S4

Statistics for **Figs. 3j – 3l**: 3-way ANOVA with factors of “Time”, "Encapsulation" and "Order".

Source	Nparm	DF	Sum of Squares	F Ratio	Prob > F
Time	1	1	3612860	3.7024	0.061
Encapsulation	1	1	20048169	20.5452	<.0001
Order	2	2	218970231	112.1994	<.0001

Table S5

Statistics for **Fig. 3j**: 2-way ANOVA with factors of "Time" and "Encapsulation".

Source of Variation	% of total variation	P value	P value summary	Significant?
Interaction	1.308	0.2853	ns	No
Time	13.82	0.0034	**	Yes
Encapsulation	72.32	< 0.0001	****	Yes

Sidak's multiple comparisons test after the ANOVA

	Mean Diff.	95% CI of diff.	Significant?	Summary	Adjusted P Value
Solution - Liposome					
1h	2959	1474 to 4444	Yes	***	0.0005
3h	3879	2394 to 5364	Yes	****	< 0.0001

Table S6

Statistics for **Fig. 3k**: 2-way ANOVA with factors of "Time" and "Encapsulation".

Source of Variation	% of total variation	P value	P value summary	Significant?
Interaction	0.7342	0.5091	ns	No
Time	4.334	0.1241	ns	No
Encapsulation	75.91	< 0.0001	****	Yes

Sidak's multiple comparisons test after the ANOVA

	Mean Diff.	95% CI of diff.	Significant?	Summary	Adjusted P Value
Solution - Liposome					
1h	453.5	238.1 to 669.0	Yes	***	0.0003
3h	372.3	156.9 to 587.8	Yes	**	0.0017

Table S7

Statistics for **Fig. 3l**: 2-way ANOVA with factors of "Time" and "Encapsulation".

Source of Variation	% of total variation	P value	P value summary	Significant?
Interaction	4.032	0.4007	ns	No
Time	18.41	0.0872	ns	No
Encapsulation	13.84	0.1324	ns	No

Sidak's multiple comparisons test after the ANOVA

	Mean Diff.	95% CI of diff.	Significant?	Summary	Adjusted P Value
Solution - Liposome					
1h	70.26	-31.80 to 172.3	No	ns	0.1977
3h	21	-81.06 to 123.1	No	ns	0.8471

Table S8

Statistics for **Fig. 4b**: 2-way ANOVA with factors of "firefly or Renilla" and "alpha-Hemolysin Combination".

Source of Variation	% of total variation	P value	P value summary	Significant?
Interaction	34.06	< 0.0001	****	Yes
alpha-Hemolysin Combination	43.87	< 0.0001	****	Yes
firefly or Renilla	18.41	< 0.0001	****	Yes

Sidak's multiple comparisons test after the ANOVA. The four combinations of alpha-hemolysin (aHL) compared in this table correspond to the four clusters (of two bars each) in **Fig. 4b**. The concentrations of aHL DNA used to construct each liposome population are as follows:

aHL combination	aHL in firefly Luciferase liposomes	aHL in Renilla Luciferase liposomes
A	0.1 nM	0.1 nM
B	5 nM	5 nM
C	0.1 nM	5 nM
D	5 nM	0.1 nM

	Mean Diff.	95% CI of diff.	Significant?	Summary	Adjusted P Value
Firefly luciferase expression					
B vs. A	4730	2699 to 6761	Yes	****	< 0.0001
C vs. A	-80.77	-2112 to 1951	No	ns	> 0.9999
D vs. A	3498	1466 to 5529	Yes	***	0.0003
C vs. B	-4811	-6842 to -2780	Yes	****	< 0.0001
D vs. B	-1233	-3264 to 798.7	No	ns	0.45
D vs. C	3578	1547 to 5610	Yes	***	0.0002

Renilla luciferase expression					
B vs. A	10890	8859 to 12921	Yes	****	< 0.0001
C vs. A	9855	7824 to 11886	Yes	****	< 0.0001
D vs. A	-246.6	-2278 to 1785	No	ns	0.9996
C vs. B	-1035	-3066 to 996.4	No	ns	0.6416
D vs. B	-11137	-13168 to -9105	Yes	****	< 0.0001
D vs. C	-10102	-12133 to -8070	Yes	****	< 0.0001

Table S9

Statistics for **Fig. S13b**: 2-way ANOVA with factors of "Theophylline" and "Time".

Source of Variation	% of total variation	P value	P value summary	Significant?
Interaction	8.412	< 0.0001	****	Yes
Time	44.57	< 0.0001	****	Yes
Theophylline	45.6	< 0.0001	****	Yes

Sidak's multiple comparisons test after the ANOVA

	Mean Diff.	95% CI of diff.	Significant?	Summary	Adjusted P Value
+ Theo					
1 vs. 0	226.3	138.7 to 313.9	Yes	****	< 0.0001
2 vs. 0	425.5	337.9 to 513.1	Yes	****	< 0.0001
3 vs. 0	571	483.4 to 658.6	Yes	****	< 0.0001
4 vs. 0	661.8	574.2 to 749.4	Yes	****	< 0.0001
5 vs. 0	693.7	606.1 to 781.3	Yes	****	< 0.0001
6 vs. 0	774.6	687.0 to 862.2	Yes	****	< 0.0001
7 vs. 0	872.3	784.7 to 959.9	Yes	****	< 0.0001
8 vs. 0	889	801.4 to 976.6	Yes	****	< 0.0001
9 vs. 0	953.3	865.7 to 1041	Yes	****	< 0.0001
10 vs. 0	963.8	876.2 to 1051	Yes	****	< 0.0001
- Theo					
1 vs. 0	55.64	-31.96 to 143.2	No	ns	0.5177
2 vs. 0	109.1	21.53 to 196.7	Yes	**	0.0059
3 vs. 0	181.2	93.57 to 268.8	Yes	****	< 0.0001
4 vs. 0	217	129.4 to 304.6	Yes	****	< 0.0001
5 vs. 0	256.2	168.6 to 343.8	Yes	****	< 0.0001
6 vs. 0	294.4	206.8 to 382.0	Yes	****	< 0.0001
7 vs. 0	309.6	222.0 to 397.2	Yes	****	< 0.0001
8 vs. 0	337.4	249.8 to 425.0	Yes	****	< 0.0001
9 vs. 0	345.4	257.8 to 433.0	Yes	****	< 0.0001
10 vs. 0	368.8	281.2 to 456.4	Yes	****	< 0.0001

Table S10

Statistics for **Fig. S13d**: 2-way ANOVA with factors of "Arabinose" and "Time".

Source of Variation	% of total variation	P value	P value summary	Significant?
Interaction	17.39	< 0.0001	****	Yes
Time	17.5	< 0.0001	****	Yes
Arabinose	63.1	< 0.0001	****	Yes

Sidak's multiple comparisons test after the ANOVA

	Mean Diff.	95% CI of diff.	Significant?	Summary	Adjusted P Value
+ Ara					
1 vs. 0	253.7	-99.71 to 607.1	No	ns	0.3454
2 vs. 0	675.2	321.8 to 1029	Yes	****	< 0.0001
3 vs. 0	1332	978.8 to 1686	Yes	****	< 0.0001
4 vs. 0	1838	1484 to 2191	Yes	****	< 0.0001
5 vs. 0	2117	1764 to 2471	Yes	****	< 0.0001
6 vs. 0	2232	1879 to 2586	Yes	****	< 0.0001
7 vs. 0	2261	1908 to 2615	Yes	****	< 0.0001
8 vs. 0	2344	1991 to 2698	Yes	****	< 0.0001
9 vs. 0	2464	2110 to 2817	Yes	****	< 0.0001
10 vs. 0	2480	2126 to 2833	Yes	****	< 0.0001
- Ara					
1 vs. 0	0.5058	-352.9 to 353.9	No	ns	> 0.9999
2 vs. 0	1.534	-351.9 to 354.9	No	ns	> 0.9999
3 vs. 0	2.061	-351.4 to 355.5	No	ns	> 0.9999
4 vs. 0	2.881	-350.5 to 356.3	No	ns	> 0.9999
5 vs. 0	3.41	-350.0 to 356.8	No	ns	> 0.9999
6 vs. 0	2.614	-350.8 to 356.0	No	ns	> 0.9999
7 vs. 0	3.177	-350.2 to 356.6	No	ns	> 0.9999
8 vs. 0	3.376	-350.0 to 356.8	No	ns	> 0.9999
9 vs. 0	4.785	-348.6 to 358.2	No	ns	> 0.9999
10 vs. 0	4.89	-348.5 to 358.3	No	ns	> 0.9999

Table S11

Statistics for **Fig. 6**: 3-way ANOVA with factors of "Mechanism", "Occupancy A", "Occupancy B", and "SNARE compatibility". (i.e., whether the SNARE protein mimics are complementary, equal, or not present).

Source	Nparm	DF	Sum of Squares	F Ratio	Prob > F
Mechanism	4	4	1878842.8	6.1006	<.0001
Occupancy A	2	2	3944276.1	25.6142	<.0001
Occupancy B	2	2	4663508.3	30.2849	<.0001
SNARE Type	2	2	3745780.4	24.3251	<.0001

Literature

1. Crabb, D. W. & Dixon, J. E. A method for increasing the sensitivity of chloramphenicol acetyltransferase assays in extracts of transfected cultured cells. *Anal. Biochem.* **163,** 88–92 (1987).

2. Sun, Z. Z., Hayes, C. A., Shin, J., Caschera, F., Murray, R. M., Noireaux, V. Protocols for Implementing an *Escherichia coli* Based TX-TL Cell-Free Expression System for Synthetic Biology. *J. Vis. Exp.* (79), e50762, doi:10.3791/50762 (2013)

3. Stano, P. & Luisi, P. L. Semi-synthetic minimal cells: Origin and recent developments. *Curr. Opin. Biotechnol.* **24,** 633–638 (2013).

4. Agapakis, C. M. Designing Synthetic Biology. *ACS Synth. Biol.* **3,** 121–128 (2014).

5. Adamala, K. *et al.* Open questions in origin of life: experimental studies on the origin of nucleic acids and proteins with specific and functional sequences by a chemical synthetic biology approach. *Comput. Struct. Biotechnol. J.* **9,** e201402004 (2014).

6. Porcar, M. *et al.* The ten grand challenges of synthetic life. *Syst. Synth. Biol.* **5,** 1–9 (2011).

7. Naylor, L. H. Reporter gene technology: the future looks bright. *Biochem. Pharmacol.* **58,** 749–757 (1999).

8. Hakkila, K., Maksimow, M., Karp, M. & Virta, M. Reporter Genes lucFF, luxCDABE, gfp, and dsred Have Different Characteristics in Whole-Cell Bacterial Sensors. *Anal. Biochem.* **301,** 235–242 (2002).

9. Choy, G. *et al.* Comparison of noninvasive fluorescent and bioluminescent small animal optical imaging. *Biotechniques* **35,** 1022–1030 (2003).

10. Hall, M. P. *et al.* Engineered luciferase reporter from a deep sea shrimp utilizing a novel imidazopyrazinone substrate. *ACS Chem. Biol.* **7,** 1848–1857 (2012).

11. Lentini, R. *et al.* Integrating artificial with natural cells to translate chemical messages that direct E. coli behaviour. *Nat. Commun.* **5,** 4012 (2014).

12. Lentini, R. *et al.* Fluorescent Proteins and in Vitro Genetic Organization for Cell-Free Synthetic Biology. (2013).

13. Lewis, B. a & Engelman, D. M. Lipid bilayer thickness varies linearly with acyl chain length in fluid

phosphatidylcholine vesicles. *J. Mol. Biol.* **166,** 211–217 (1983).

14. Nezil, F. a. & Bloom, M. Combined influence of cholesterol and synthetic amphiphillic peptides upon bilayer thickness in model membranes. *Biophys. J.* **61,** 1176–1183 (1992).

15. Jousma, H. *et al.* Characterization of liposomes. The influence of extrusion of multilamellar vesicles through polycarbonate membranes on particle size, particle size distribution and number of bilayers. *Int. J. Pharm.* **35,** 263–274 (1987).

16. Olson, F., Hunt, C. a, Szoka, F. C., Vail, W. J. & Papahadjopoulos, D. Preparation of liposomes of defined size distribution by extrusion through polycarbonate membranes. *Biochim. Biophys. Acta* **557,** 9–23 (1979).

17. Berger, N., Sachse, a., Bender, J., Schubert, R. & Brandl, M. Filter extrusion of liposomes using different devices: Comparison of liposome size, encapsulation efficiency, and process characteristics. *Int. J. Pharm.* **223,** 55–68 (2001).

18. Caschera, F. & Noireaux, V. Compartmentalization of an all-E. coli Cell-Free Expression System for the Construction of a Minimal Cell. Artif. Life 22, 185-95 (2016).

19. Kamat, N. P. *et al.* Electrostatic Localization of RNA to Protocell Membranes by Cationic Hydrophobic Peptides. *Angew. Chemie - Int. Ed.* **54,** 11735–11739 (2015).

20. McAdams, H. H. & Arkin, a. Simulation of prokaryotic genetic circuits. *Annu. Rev. Biophys. Biomol. Struct.* **27,** 199–224 (1998).

21. Purnick, P. E. M. & Weiss, R. The second wave of synthetic biology: from modules to systems. *Nat. Rev. Mol. Cell Biol.* **10,** 410–422 (2009).

22. Shin, J. & Noireaux, V. An E. coli cell-free expression toolbox: Application to synthetic gene circuits and artificial cells. *ACS Synth. Biol.* **1,** 29–41 (2012).

23. Brödel, A. K. & Kubick, S. Developing cell-free protein synthesis systems: a focus on mammalian cells. *Pharm. Bioprocess.* **2,** 339–348 (2014).

24. Chang, H. C., Kaiser, C. M., Hartl, F. U. & Barral, J. M. De novo folding of GFP fusion proteins: High efficiency in eukaryotes but not in bacteria. *J. Mol. Biol.* **353,** 397–409 (2005).

25. Hillebrecht, J. R. & Chong, S. A comparative study of protein synthesis in in vitro systems: from the prokaryotic reconstituted to the eukaryotic extract-based. *BMC Biotechnol.* **8,** 58 (2008).

26. Sun, Z. Z. *et al.* Protocols for Implementing an Escherichia coli Based TX-TL Cell-Free Expression System for Synthetic Biology. *J. Vis. Exp.* 1–15 (2013). doi:10.3791/50762

27. Caschera, F. & Noireaux, V. A cost-effective polyphosphate-based metabolism fuels an all E. coli cell-free expression system. *Metab. Eng.* **27,** 29–37 (2015).

28. Garamella, J., Marshall, R., Rustad, M. & Noireaux, V. The all E. coli TX-TL Toolbox 2.0: a platform for cell-free synthetic biology. ACS Synth. Biol. 5, 3044-30445. acssynbio.5b00296 (2016). doi:10.1021/acssynbio.5b00296

29. Liu, D. V., Zawada, J. F. & Swartz, J. R. Streamlining Escherichia Coli S30 extract preparation for economical cell-free protein synthesis. *Biotechnol. Prog.* **21,** 460–465 (2005).

30. Kigawa, T. *et al.* Preparation of Escherichia coli cell extract for highly productive cell-free protein expression. *J Struct Funct Genomics* **5,** 63–68 (2004).

31. Machida, K., Masutan, M. & Imataka, H. Protein Synthesis in vitro: Cell-Free Systems Derived from Human Cells. (2012). doi:10.5772/48563

32. Mikami, S., Kobayashi, T., Masutani, M., Yokoyama, S. & Imataka, H. A human cell-derived in vitro coupled transcription/translation system optimized for production of recombinant proteins. *Protein Expr. Purif.* **62,** 190–198 (2008).

33. Xu, C., Hu, S. & Chen, X. Artificial cells: from basic science to applications. Mater. Today 00, 1-17. (2016).

34. Caschera, F. & Noireaux, V. Integration of biological parts toward the synthesis of a minimal cell. *Curr. Opin. Chem. Biol.* **22,** 85–91 (2014).

35. Mikami, S., Masutani, M., Sonenberg, N., Yokoyama, S. & Imataka, H. An efficient mammalian cell-free translation system supplemented with translation factors. *Protein Expr. Purif.* **46,** 348–57 (2006).

36. Chen, I. a. & Szostak, J. W. A Kinetic Study of the Growth of Fatty Acid Vesicles. *Biophys. J.* **87,** 988–998 (2004).

37. Chen, I. a., Salehi-Ashtiani, K. & Szostak, J. W. RNA catalysis in model protocell vesicles. *J. Am. Chem. Soc.* **127,** 13213–13219 (2005).